KU LEUVEN

FACULTEIT GENEESKUNDE
BIOMEDISCHE WETENSCHAPPEN

VIRTUELE PATHOLOGIE VAN PROSTAATKANKERSTALEN MET MRI

Virtual pathology of prostate cancer samples using MRI

Masterproef voorgedragen tot het behalen van de graad van Master in de biomedische wetenschappen door
Mary GLORIEUX

Promotor: Prof. dr. Uwe Himmelreich
Biomedical MRI unit
Departement Pathologie en Beeldvorming

Begeleider: dr. Willy Gsell
Biomedical MRI unit
Departement Pathologie en Beeldvorming

Leuven, 2015-2016

KU LEUVEN

FACULTEIT GENEESKUNDE
BIOMEDISCHE WETENSCHAPPEN

VIRTUELE PATHOLOGIE VAN PROSTAATKANKERSTALEN MET MRI

Virtual pathology of prostate cancer samples using MRI

Masterproef voorgedragen tot het behalen van de graad van Master in de biomedische wetenschappen door
Mary GLORIEUX

Promotor: Prof. dr. Uwe Himmelreich
Biomedical MRI unit
Departement Pathologie en Beeldvorming

Begeleider: dr. Willy Gsell
Biomedical MRI unit
Departement Pathologie en Beeldvorming

Leuven, 2015-2016

Preface

I would like to thank all the people who made this thesis possible. First of all my supervisor dr. Willy Gsell who helped me a lot and was always willing to answer my questions. Thanks for explaining everything about MRI to me and for your support. I would also like to thank my promotor Prof. dr. Uwe Himmelreich, without him this thesis would not be possible. I am grateful that you have given me this opportunity although I am a clinical biomedical master student. I also enjoyed the nice work environment of the MoSAIC very much. The good atmosphere during the lunch moments and the lab evenings were very nice. Everyone was willing to help me for instance Kristof Govaerts helped me many times with the processing of the MRI data and all kinds of computer problems. Along with the other members of the study team made this thesis possible: Prof. dr Karin Haustermans, Ir. Frederik De Keyzer and dr. Sofie Isebaert from the lab of experimental radiology. Sofie, thank you for explaining me the practical details about the study so kindly and giving me the chance and confidence for the patient recruitment. Also Prof. dr Evelyne Lerut and Gerda Luyckx from the department of Pathology who allowed me to attend the pathological workup. Furthermore, I would like to thank Prof. Frederik Maes and dr. An Elen from the Medical Imaging Research Centre who designed the registration tool and helped me to register the data. Together with dr. Janaki Raman Rangarajan, who helped me a lot with solving all kinds of registration problems and the automatic tool to transfer the data from Bruker to the Analyze format. As well the doctors of the department of Urology: Dr. Lorenzo Tosco, Dr. Wouter Everaerts and Prof. Dr. Steven Joniau. Thank you Dr. Tosco for the very interesting internship that I could do with the study consultation team and for reading my thesis. Thank you Dr. Everaert and Prof. Joniau that I could attend the operations and inform patients at your consultations.

Next to all these people of the MoSAIC and the study team, I would like to thank my fellow thesis student and my colleague Simon Vanden Berghe very warmly. In particular Celine and Natacha for all their support and effort. Our funny moments in our cold and very crowded office, I will remember them vividly. Together with our nice dance evenings on Wednesday, the presentation evenings, barbeque moments and laughing evenings were very enjoyable. I have met two totally new girls and after these ten months of intense collaboration they will stay very good friends of me that I will never forget. Next year we need to maintain this friendship in our new apartment and the dance classes.

Most of all, I would like to thank my parents and my family, without them I would not be able to do this. Thank you for all your support and giving me the chance and confidence to study and to start my PhD next year. Especially I would like to thank my boyfriend Bram who was always there to support me, I could always call him day and night. He was willing the hear my complaints and knew perfectly how to relieve my stress. Thank you so much for all your support, confidence, compliments, your effort and love. I would like to take care of you as you took care of me for the rest of our life.

Table of contents

List of abbreviations

3D-CRT	Three-dimensional conformal radiotherapy
ADC	Apparent diffusion coefficient
ADT	Androgen deprivation therapy
AFS	Anterior fibromuscular stroma
B_0	Primary magnetic field
BPH	Benign prostate hypertrophy
CT	Computer tomography
CZ	Central zone
DCE	Dynamic contrast enhanced
DRE	Digital rectal examination
DWI	Diffusion weighted imaging
EAU	European Association of Urology
EBRT	External beam radiotherapy
ERSPC	European randomized study of screening for prostate cancer
FA	Fractional Anisotropy
H&E	Hematoxylin and Eosin
HIFU	High intensity focal ultrasound
HPC	Hereditary prostate cancer
IMRT	Intensity-modulated radiotherapy
LRP	Laparoscopic radical prostatectomy
mpMRI	Multiparametric magnetic resonance imaging
MRI	Magnetic resonance imaging
PCa	Prostate cancer
PCOS	Prostate cancer outcomes study
PLCO	Prostate, Lung, Colorectal and Ovary study
PSA	Prostate specific antigen
PSA DT	Prostate specific antigen doubling time
PSA3	Prostate specific antigen 3
PSAV	Prostate specific antigen velocity
PZ	Peripheral zone
RALP	Robot assisted laparoscopic prostatectomy
RF pulse	Radio frequent pulse
ROI	Region of interest
RRP	Retropubic radical prostatectomy
T2w	T2 weighted imaging
TRUS	Transrectal ultrasound

Abstract

Introduction:

Prostate cancer (PCa) is the most common non-skin cancer in men. Multiparametric magnetic resonance imaging (mpMRI) can identify and localize PCa non-invasively, in contrast to transrectal ultrasound-guided biopsies. mpMRI has improved sensitivity and specificity to detect PCa compared to T1, T2, diffusion weighted and dynamic contrast enhanced MRI scans separately due to combined anatomical and functional information. The aim of the study was thus to determine *in vivo* MRI biomarkers for low grade PCa through correlation with *ex vivo* MRI and histopathology.

Materials and Methods:

Fourteen low grade PCa patients were prospectively included in the Dr. Therapat study. Two *in vivo* mpMRI scans (3T) were performed whereby a patient-specific, 3D-printed mold of the prostate was generated. The prostate was scanned *ex vivo* using high-resolution MRI at 9.4T. H&E slides were obtained by whole-mount histology as gold standard. All images were acquired in the same plane thanks to the mold design. MR images were then registered with histology data to determine T2, apparent diffusion coefficient (ADC) and fractional anisotropy (FA) values as potential biomarkers.

Results:

ADC values were significantly lower in cancerous than healthy tissue in the transition zone ($p<0.0001$). FA was significantly lower in cancerous than healthy tissue in both transition and peripheral zone.

Conclusion:

The 3D printed mold enabled a one-to-one registration of histology to MRI data. This registration step needs further validation, which is essential for the identification of biomarkers and for implementation of mpMRI in treatment management of low grade PCa. More patient data are required for large scale validation.

1. Introductory literature overview

1.1. Wide problem formulation

Prostate cancer (PCa) is the most common non-skin cancer amongst men in Europe. Almost 417,000 cases were estimated in 2012, affecting one men out of six (1). For 2016, almost 180,890 new cases are estimated in the US and 26,120 estimated deaths (2). The most common technique used for diagnosis of PCa is transrectal ultrasound (TRUS) guided biopsy. The last decade the rise in PSA testing led to an increased use of TRUS guided biopsies. Unfortunately this technique has a poor specificity with a high rate of false negative results (10-40%) (3). Advanced imaging techniques namely magnetic resonance imaging (MRI) has the potential to address this high false negative rate of TRUS guided biopsy as it is a non-invasive tool that can visualize the prostate's anatomy and detect tumours (4). Multiparametric MRI (mpMRI) has evolved this latest years to the most promising modality to characterize prostate tissue, because it combines high-resolution anatomic information of T2 weighted (T2w) images with the regional diffusion characteristics of diffusion weighted imaging (DWI) (4). That is why mpMRI can be used as imaging modality in image-guided targeted biopsies, planning surgical procedures, optimal planning of treatment, evaluation and follow-up of PCa (4). Currently mpMRI is already implemented in clinical practice mostly for high grade tumours but to achieve the same knowledge for low grade tumours, further research is necessary. Until now the mpMRI is not yet standard of care in the European Association of Urology (EAU) guidelines of 2015 and therefore the MRI findings need to be confirmed by histological findings (4). Whole-mount histology is the gold standard to evaluate the accuracy of the imaging test, and these whole-mount histology samples are obtained by radical prostatectomy which is one of the conventional curative therapy for PCa. However, the *in vivo* detection of pathologic sites of cancer remains a significant challenge (5). In this study patients with low grade PCa were recruited from the EC FP7 project, 'Dr Therapat project'. Today the problem is not to diagnose PCa but to distinguish tumours that require aggressive therapy from those where active follow-up is more appropriate. Most man die with PCa but not from PCa and that is why an appropriate treatment management is necessary. Therefore, the focus of the study was laid on low grade PCa patients to see if there is a correlation between *in vivo* MRI and histology. The aim is to see if a biomarker can be identified for the detection of low grade tumours on mpMRI and what can be done to increase the sensitivity of the mpMRI technique.

Furthermore, the purpose is to register the *in vivo* MR images to histological sections to improve the predictive value of mpMRI. A patient-specific, 3D printed mold together with high resolution *ex vivo* MR images are tested to make an accurate registration between all the acquired images possible. Successful co-registration could improve mpMRI for the localization of tumour nodules and estimation of the lesion volume for low grade PCa.

1.2. Epidemiology

PCa is the sixth most common cancer in the world and the second most prevalent cancer in men, affecting one men out of six (6). In Europe close to 400.000 new cases have been diagnosed in 2015 (7), thereby outnumbering lung and colorectal cancer (8). There are large regional differences in incidence rates of PCa in Europe, ranging from 68.8 cases per 1000 men in Malta to 182 in Belgium (8). In Flanders, PCa is the most diagnosed cancer in men with 7909 invasive cancers diagnosed in 2013 with an average age of 69.2 (9). Almost 3 men out of 100 die of PCa, mostly above the age of 70. The 5-year survival rate for men in Europe steadily increased from 73.4% in 1999-2001 to 83.4% in 2005-2007 (10), which is significantly lower than in the United States where it was 99.3% (11). These numbers indicate the widespread burden of PCa and emphasize the importance of a good diagnosis and management of the disease.

1.2.1. Risk factors

The risk factors of developing clinical PCa are not fully known, although three well-established risk factors have been identified: heredity, increasing age and ethnicity (8).

1.2.1.1. Heredity

Hereditary susceptibility is considered as the strongest risk factor for PCa. If one first-line relative has the disease, the risk is at least doubled (12). Epidemiological studies indicated that 5-10% of all PCa cases are caused by dominantly inherited susceptibility genes (12). The risk is greater for brothers than for sons, and this risk increases when the cancer is diagnosed early in the family. That is why family history of PCa must always be part of the anamnesis (12). A locus on the long arm of chromosome 1 (1q24-25) was named hereditary prostate cancer gene 1 (HPC1) and was suggested as the putative PCa susceptibility gene. However, different other genes were found to be involved in the disease: HPC1 on 1q24-25, PCa gene on 1q42-43, HPCX on the X-chromosome, CAPB on 1p36 and HPC2 on 17p12. These genes are found in studies in different populations, but the problem is that other studies have failed to confirm these loci. Until now no clinically important prostate susceptibility genes have been identified or cloned, therefore the diagnosis of hereditary PCa is still based on a pedigree analysis. That these genes are not identified or cloned yet, is possibly due to the difficulties of cloning the hereditary prostate cancer (HPC) genes, or to the complex genetics of hereditary PCa (13).

1.2.1.2. Age

PCa is rarely diagnosed in men younger than 40 years old. The mean age of patients is 72-74 years and about 85% of the patients are diagnosed after the age of 65 as shown in Figure 1 (14,15). Therefore, PCa is a bigger health concern in developed countries (10).

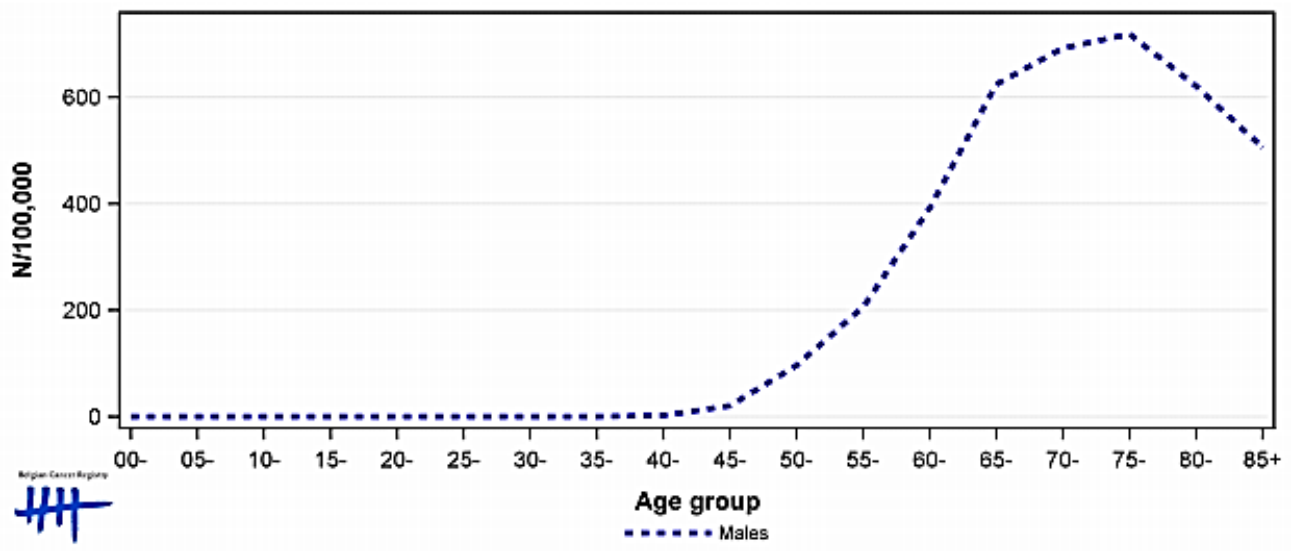

Figure 1. Age-standardized Incidence rate of prostate cancer in Belgium in 2013. Prostate cancer is rarely diagnosed before the age of 40 and 85% of the patients are diagnosed after the age of 65 (9).

1.2.1.3. Ethnicity

The incidence of PCa varies between ethnic populations and countries. The lowest rates are usually in Asia and the highest are in North America and Scandinavia, especially in African-American people in the USA (137 per 100 000 per year) (14). The race is also a statistically significant predictor of high grade disease (Gleason score >7). For example African Americans have a 40% higher risk for PCa with a greater chance to develop a high grade condition in comparison to non-African American.

In general the risk factors that are the strongest associated with PCa are ethnicity (higher risk among African Americans, lower among Hispanics), family history (higher risk with a positive family history) and age (risk increases with age) (16).

1.3. Anatomy of the prostate

The prostate is the largest accessory gland of the male reproductive system. It is located posterior to the lower part of the symphysis pubis, anterior to the rectum and inferior to the bladder (Figure 2) (6). The prostate is classically described as a 'walnut-shaped' gland because of its conical shape. Furthermore, it secretes an alkaline fluid, which is a portion of the seminal fluid. This alkaline fluid ensures that the spermatozoa stay alive and movable. The prostate itself is composed of glandular and stromal tissue, surrounded by a pseudocapsule. The inner layer of this pseudocapsule consists of smooth muscle and the outer layer of collagen. The innervation comes from the prostatic plexus and the blood supply is derived from branches of the internal iliac artery (17).

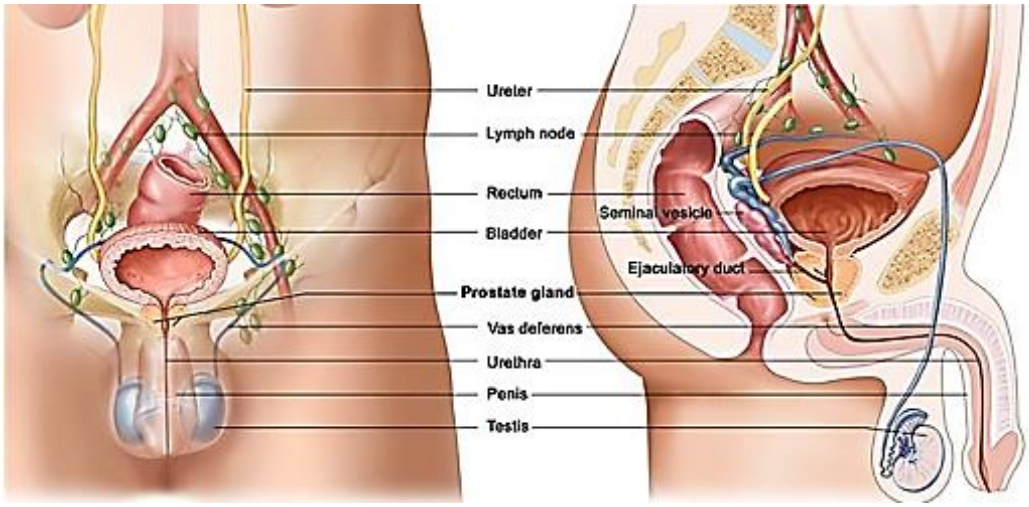

Figure 2. Anatomy of the male reproductive and urinary system. The prostate is located posterior to the lower part of the symphysis pubis, anterior to the rectum and inferior to the bladder. Adapted from (18).

The prostate is divided into four regions: the central zone (CZ), the transition zone (TZ), the peripheral zone (PZ) and the anterior fibromuscular stroma (AFS) (Figure 3). Furthermore, the prostate gland is divided into three parts: the apex, the midprostate and the base. First, the apex is the lower third part of the prostate. Secondly, the midprostate is the middle third that includes the verumontanum, which is the part where the ejaculatory ducts enter the urethra. Third, the base is the upper part of the prostate gland just below the bladder (6).

The different zones in the prostate are characterised by their own features. The PZ is the largest zone, which comprises almost 70% of the prostate. In this zone, carcinoma, chronic prostatitis and postinflammatory atrophy are more common than in other zones. The CZ accounts for 25% of the prostatic tissue. The TZ only accounts for 5% of the glandular tissue and consists of two lobules next to the proximal urethra, posterior to the verumontanum. The TZ is the part which enlarges in benign prostatic hyperplasia (BPH). The AFS is composed of fibrous and smooth muscular tissue (6).

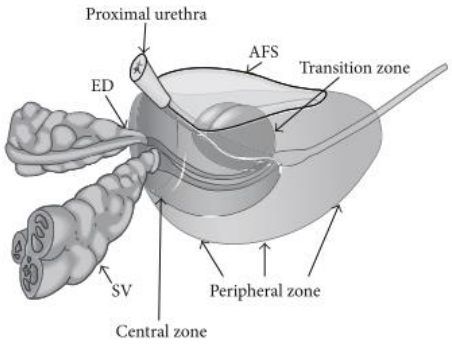

Figure 3. The prostate is divided into four zones with their own characteristics. The prostate is divided into four different zones: the central zone , the transition zone, the peripheral zone and the anterior fibromuscular stroma (AFS). ED: ejaculatory ducts; SV: seminal vesicles. Adapted from (6).

1.4. Prostate cancer screening

PCa screening is usually based on PSA detection or a digital rectal examination (DRE) (6). PSA is a protein produced by the prostate gland and is secreted in the seminal fluid and blood. The PSA level can be measured by a simple blood sample. In the last decade there were two population-based screening programs to investigate the effect of a preventive PSA screening in all men. The Prostate, Lung, Colorectal, and Ovary (PLCO) trial in the United States and the European Randomized Study of Screening for Prostate Cancer (ERSPC) in Europe. Based on the results of these studies, the major urologic societies have recommended that a widespread screening for PCa is not necessary at the moment (8,14,19). The PSA screening increased the PCa incidence and led to diagnosis of asymptomatic cancers that otherwise would not emerge during life (17).

PSA screening is known to have a low specificity (36%) (21). Therefore, several modifications have been suggested that may improve the specificity of PSA, for instance the ratio of the free PSA to the total PSA (f/t PSA) in the serum (10). This improvement results in a significant decrease in the number of unnecessary biopsies and increase in the detection rate of PCa. A major disadvantage is that several pre-analytical factors influence the f/t PSA, making it very difficult to implement it in the daily clinical workflow. PSA velocity (PSAV), PSA doubling time (PSA DT) as well as a new biomarker prostate cancer antigen 3 (PCA3) have shown no advantages compared to the traditional PSA value (8). Using exclusively these measurements is not suitable to counsel an individual patient on the need to perform a prostate biopsy to rule out PCa.

The digital rectal examination (DRE) is a test where the doctor brings his finger rectally in the patient to feel if the prostate is uneven or callous. DRE is effective for identifying posterior PZ tumours, but fails to detect many tumours that originate in the anterior PZ, CZ, and TZ as well as tumours that are too small to be palpated (19).

1.5. Diagnosis of prostate cancer

As described above, PSA screening has a low specificity even with the suggested modifications to improve this. However, due to lack of alternatives, the early detection of PCa still relies on the combination of serum PSA, DRE and TRUS guided biopsy, which is the gold standard for diagnosis of PCa according to the EAU guidelines of 2015 (8). TRUS or a transrectal ultrasound directed 18-gauge core biopsy obtains material for histopathologic examination. It is an invasive examination because multiple punctures are made of 16-18 Gauge to obtain the prostate samples in a systematic zone-based way. Ultrasound-guided periprostatic nerve block is a state of the art, simple and cost effective method that can control the pain accompanied with this invasive procedure (22). TRUS guided biopsies may underestimate the grade and extent of PCa (21,23). Therefore, the number of cores that are taken, was increased from 6 to 12 , improving the cancer detection rate. On baseline

biopsies, the sample sites should be taken as far posterior and lateral as possible in the peripheral gland. Additional cores can be obtained from suspect areas by DRE/TRUS. TRUS guided biopsy is indicated for patients with an elevated PSA level and an abnormal DRE. Nowadays a cut-off of 4 ng/ml PSA is traditionally used, although PCa is possible at any PSA level (21). The age of the patient and possible comorbidities are also taken into account to possibly perform a TRUS guided biopsy. The decision to proceed with further diagnostic or staging examinations is guided by the treatment options available for the patient, taking the patients preference, age, and comorbidity into consideration (Table 1). The role of mpMRI in the diagnosis of PCa will be discussed later on.

Table 1. Diagnostic and staging examinations advised per prostate cancer risk. Adapted from (7,10)**.**

Prostate cancer risk	*Diagnostic or staging workup advised*
Low risk PCa	Imaging tests are not routinely recommended.
Intermediate risk PCa	Bone scintigraphy should be considered if bone metastases are suspected clinically, if the Gleason score is >(4 + 3) or serum PSA is >15 ng/ml. A bone scan and cross-sectional imaging is required.
High risk PCa	mpMRI should be used for staging, together with CT/MRI and bone scintigraphy.

1.6. Classification and staging systems

PCa is mostly classified in three ways, namely based on: the PSA level, the TNM classification and the Gleason score.

1.6.1. PSA value

PSA was introduced in 1980 as an accurate serum biomarker for PCa (24). Nowadays, PSA is considered as a prostate tissue marker to monitor response to therapy and disease progression. When the PSA value rises, it is important to know how much it rises and in which time period. Elevated PSA levels may indicate PCa (Table 2), but numerous noncancerous conditions, such as prostatitis or a benign prostate hypertrophy, can also cause this elevation (24).

Table 2. Prostate cancer risk related to low PSA levels (10)**.**

PSA level (ng/ml)	*Risk of PCa (%)*
0.0-0.5	6.6
0.6-1.0	10.1
1.1-2.0	17.0
2.1-3.0	23.9
3.1-4.0	26.9

1.6.2. TNM classification

The TNM classification indicates how far the tumour has spread. This TNM classification has been introduced by the American Joint Committee on Cancer (AJCC) and the Union for International Cancer Control (UICC) in 1997 (6). T stands for tumour, four options can be chosen in this subcategory, dependently on the size and spreading of the cancer. N stands for lymph nodes to see if there are affections of the lymph nodes. M stands for metastases and depends on the location of the metastases (Table 3). To determine the TNM stage, different tests need to be done to see how far the tumour has spread. To assess the T stage, histopathological samples need to be obtained either via TRUS guided biopsies or via prostatectomy. A bone scan, MRI, CT and ultrasound are examples of tests whereby the N and M stage can be determined. PCa at an early stage includes TNM classes T1 and T2. The classes T3a, T3b, T4, N+ and M+ are considered as late stage PCa (6).

Table 3. The TNM staging system adapted from (10,25)**.**

TNM classification	
T1	Clinically inapparent tumour, not palpable or visible by imaging
T1a	Tumour incidental on histological finding is 5% or less of the resected tissue
T1b	Tumour incidental on histological finding is more than 5% of resected tissue
T1c	Tumour identified by needle biopsy (e.g. because of elevated PSA level)
T2	The tumour is big enough to feel or see it, but it is still in the capsule
T2a	Tumour involves one half of one lobe or less
T2b	Tumour involves more than one half of one lobe, but not both lobes
T2c	Tumour involves both lobes
T3	The tumour has grown through the capsule
T3a	Extracapsular extension, unilateral or bilateral, including microscopic bladder neck involvement
T3b	The tumour is spread out to the seminal vesicles
T4	The tumour is spread out to the surrounding organs: the bladder neck, rectum and rectal sphincter
N+	The tumour is spread out to the regional lymph nodes
M+	The tumour is spread out to other organs
M1a	Non-regional lymph node(s)
M1b	Bone(s)
M1c	Other site(s)

1.6.3. Gleason score

The Gleason score has proven to be the best biomarker predicting tumour aggressiveness, disease outcome and mortality risk of PCa (26). This technique is the histological reference standard for grading PCa and is determined based upon histopathological samples usually obtained via TRUS guided biopsies. The Gleason score is based on the two most common architectural patterns in the prostate gland. These patterns can have a score from one to five, with one the least differentiated and five the most differentiated tissue (Figure 4). The more differentiated, the less the cancerous tissue resembles to the native tissue, the worse the prognosis (Table 4). The sum of the two most prevalent patterns is used because PCa is a multifocal disease and is heterogeneous, which means that prostate carcinoma can have multiple patterns (27). If the grade comprises less than 5% of the cancer lesion, it is not incorporated in the Gleason score (10).

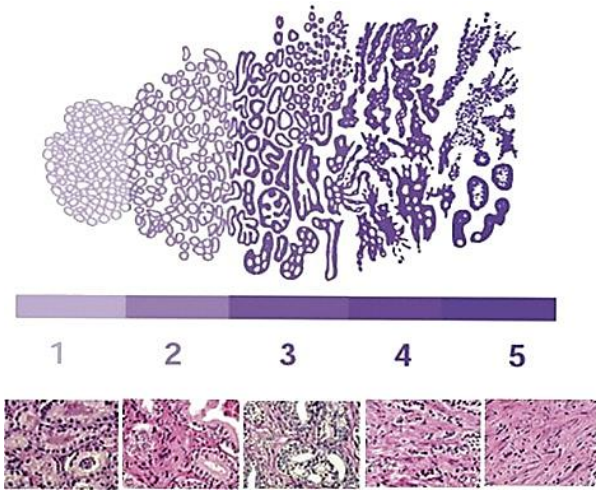

Figure 4. The Gleason score. Gleason patterns can have a score from 1 to 5, with 1 the least differentiated and 5 the most differentiated tissue compared to native tissue. The more differentiated, the worse the prognosis. The Gleason score is a sum of the 2 most prevalent patterns. Adapted from (78).

Table 4. Gleason score with respect to tumour aggressiveness adapted from (15) **with** (29) **as reference.**

Gleason Sum Score	
2-5	Low grade. The tumour probably grows slow
6-7	Intermediate grade. The tumour probably grows at an average speed
8-10	High grade. The tumour probably grows fast

Overall, three classification systems are important for PCa: the PSA level, the TNM classification system and the Gleason score. In Table 5 these three systems are summarized regarding the different PCa stages.

Table 5. Table summarizing the risk of prostate cancer based upon the PSA value, Gleason score and TNM classification for all prostate cancer stages. (10,17,24)**.**

Concluding Table

Low risk	PSA <10 ng/mL, and Gleason score <7, and clinical stage cT1–T2a	**Localised**
Intermediate risk	PSA 10–20 ng/mL, or Gleason score 7, or clinical stage T2b	
High risk	PSA >20 ng/mL, or Gleason score >7, or clinical stage >T2c	
	Any PSA value, any Gleason score, T3-4 or N+	**Locally advanced**

1.7. *Treatment of prostate cancer*

Therapeutic management of PCa has become more complex last decade because there are different stage-specific therapeutic options available. The treatment choice is influenced by the PSA-level, TNM classification, Gleason score, age, possible coexisting medical problems and by considering side effects (14). It is advised to counsel patients with low risk PCa or intermediate-risk PCa in an interdisciplinary setting with an urologist together with a radiation oncologist (20). For patients with a high-risk PCa, it is advisable to discuss neoadjuvant and adjuvant treatment options with the patients and with members of a multidisciplinary tumour board (8). As mentioned above, there are multiple therapeutic options available and no treatment is superior, which makes it difficult to choose the most appropriate treatment. There is also no consensus as what is the optimal management. Patients should be informed of the potential benefits and harms of the possible treatment options as these may cause sexual dysfunction, infertility or incontinence. The patients should also have the opportunity to consult with both a surgical- and radiation oncologist (20). To help the patients in the decision-making process, they can be documented with decision-making guidelines. Although there is a lack of randomized-controlled trials in this field, some recommendations can be made, based on the literature (10). Below the possible treatment options will be discussed (8).

1.7.1. Active surveillance

Active surveillance is a suitable therapy for patients with low risk PCa that do not require immediate intervention (30). These patients are also candidates for a curative approach, but these low risk tumours mostly have an indolent course and grow slow, which allows follow-up. The patient can choose to be not treated initially, but followed with a curative intent. If progression or the threat of progression occurs during follow-up, the patient will be treated but side effects of radical treatment are initially avoided (30). Active surveillance was introduced with the aim to reduce the ratio of overtreatment in patients with low risk PCa. Men with a life expectancy >10 year and low risk PCa are good candidates for active surveillance (10). Only about 30% of men will require delayed radical intervention. Eligibility criteria for active surveillance are developed by different studies (8,10), including:

- Clinically confined PCa (T1c–T2)
- Gleason score ≤ 6
- ≤ 2 biopsies involved with cancer
- ≤ 50% of each positive biopsy core involved with cancer
- PSA ≤ 10 ng/ml

For active surveillance the patient needs to be tested regularly, which includes: blood sampling, ultrasound and biopsies to see how the tumour has grown, changed or spread (31). Active surveillance protocols vary by institution but in general they rely on PSA level, DRE and TRUS guided biopsy (30). MRI can be a very useful tool for active surveillance, this will be discussed in the next section. PSA is not significantly associated with PCa progression (32). This non-association indicates the need for annual repeated biopsies to monitor men adequately under active surveillance. For example, biopsy progression is considered as a Gleason score >7, more than two positive cores at re-biopsy, or >50% core involvement (8).

The advantage of active surveillance is that the side effects associated with active therapy are postponed, but the patient is able to step into active therapy at any time. Another advantage is that it reduces the medical costs for the society. The disadvantages of this therapeutic option are that it can be too late to start therapy if the tumour spreads silently. Symptoms can start while waiting and it may cause psychological distress for the patient (10).

1.7.2. Watchful Waiting

Watchful waiting is a delayed symptomatic non-curative treatment in patients who are no candidates for an aggressive local therapy (8). This can be patients with a limited life expectancy or older patients with less aggressive cancer (10). Watchful waiting is different from active surveillance as there is less intensive follow-up and fewer tests are done, as indicated in Table 6. Due to less follow-up than active surveillance, the patient is going to progress and interventions are needed in case of symptoms. WW can be complemented with delayed hormonal therapy if there is symptomatic progression (8,10).

In the study of Rider *et al.*, the PCa mortality in patients that were treated with non-curative intent was correlated with the risk category. PCa mortality rates varied 10-fold according to the risk category (Table 5). High risk patients and advanced disease were correlated with a substantially higher mortality risk, especially in younger men with comorbidities that died mostly from cardiovascular death or other causes (33).

Table 6. Difference between active surveillance and watchful waiting, adapted from (10)**.**

	Active Surveillance	*Watchful Waiting*
Treatment intent	Curative	Palliative
Follow-up	Predefined schedule	Patient-specific
Assessment/markers used	DRE, PSA, re-biopsy, optional MRI	Not predefined
Life expectancy	>10 years	< 10 years
Aim	Minimise treatment-related toxicity without compromising survival	Minimise treatment-related toxicity

1.7.3. Radical Prostatectomy

Radical prostatectomy is a procedure in which the whole prostate is removed together with the seminal vesicles and often bilateral pelvic lymph nodes (in intermediate risk patients with a risk >5% of lymph node development or in high risk patients). Radical prostatectomy is the only treatment for localised PCa that showed a cancer-specific survival benefit when compared with watchful waiting in a prospective randomised trial (34). A nerves sparing procedure can be performed so that the periprostatic neurovascular bundle is spared to avoid erectile dysfunction. However, sometimes this is not possible because the cancer has grown into the neurovascular bundle. Three methods can be performed to remove the prostate entirely: retropubic radical prostatectomy (RRP), laparoscopic radical prostatectomy (LRP) and robot-assisted laparoscopic prostatectomy (RALP). De Carlo *et al.* compared the different operation techniques (35). With regard to the perioperative outcome, RRP was less time consuming then RALP and LRP. However, when they zoomed in on blood loss and complication rates, the laparoscopic approaches had the best overall results. Especially RALP scored high when the functional and oncological results were taken into account (35). As RALP was the surgical method of choice for low grade tumours at UZ Leuven, this technique was used for all patients in this study.

The advantages of radical prostatectomy are that the cancer is locally removed and there is a big chance to cure (8). It also gives the opportunity for detailed histological evaluation, because pathology is the gold standard in cancer diagnosis, prognosis, tissue characterization and surgical staging (4,6). On the other hand, there are always risks that are accompanied with a surgical operation, e.g. haemorrhages, infection, blood clots that can induce phlebitis or a pulmonary embolism. Fortunately, these blood clots can be prevented by anticoagulation agents for one month. Still, men can die of the operation, mostly due to unknown heart and lung problems. The disadvantages specifically for a RALP procedure are: urine retention problems, impotence and incontinence for urine or stool. A recent systematic review demonstrated that there was no evidence of differences in urinary incontinence at 12 months between LRP and RALP procedures (10). In the Prostate Cancer Outcomes Study (PCOS), 8.7% of men had a lack of urinary control and 41.9% reported sexual dysfunction after radical prostatectomy at two years. Recovery from sexual dysfunction and urinary incontinence occurs over two to three years (10). Surgical expertise influences the complication rates a lot, moreover RALP is a recent technique so there is not much evidence yet about the long-term outcome.

1.7.4. Radiation Therapy

There are two types of radiation therapy: external beam radiotherapy and internal radiotherapy, also called brachytherapy. The radiation dose depends on the PCa risk degree and histological properties of the tumour (36). High cell densities in the tumour require high radiation doses. Three-dimensional conformal radiotherapy (3D-CRT) was the gold standard radiotherapy a few years ago. However, intensity-modulated radiotherapy (IMRT), which is an optimised form of 3D-CRT, is the gold standard nowadays for external beam radiotherapy (8,10).

The choice for radiotherapy is decided multidisciplinary, based upon:

- The extent of the tumour (TNM classification)
- Gleason score
- Baseline PSA
- Age
- Comorbidity, life-expectancy and quality of life
- The preference of the patient

In the external beam radiotherapy (EBRT), the radiation is administered extern from the body. Several randomised studies showed that dose escalation ranging from 74-80 Gy had a significant impact on 5-year survival (10). This results in an everyday session of 20 minutes for seven to eight weeks. The disadvantages of EBRT is that the whole-gland dose escalation is limited due to the high probability of normal tissue complications (37).

In the second type, the internal radiotherapy or brachytherapy, radioactive seeds are implanted in the prostate. The advantage of brachytherapy is that the irradiation is administered very locally. The aim is that the side effects related to whole-gland treatment are reduced, by ablating the tumour lesion selectively and sparing the surrounding non-malignant parenchyma and organs at risk at the same time (37). However, brachytherapy is a more recent technique and that is why the long-term side effects or results are not known yet. All the patients that can have internal irradiation can also have external irradiation, but not vice versa because for the administration of brachytherapy the patient need to fulfil following conditions (10):

- Volume of the prostate must be <50 gram
- Stage T1b-T2a, M0, N0
- Gleason score <6
- PSA-level <10 ng/ml
- No or little complaints about urine retention

The advantage of radiation therapy is that, in contrast to all-or-nothing therapies as surgery, it is possible in radiotherapy to sculpt the radiation dose based on underlying tissue characteristics to obtain optimal tumour control probability (36). The side effects of radiation therapy are that it may cause urinary, bowel and sexual dysfunction. (10).

EBRT as well as brachytherapy cause irradiative voiding symptoms as urinary urgency and frequency, which causes an overall negative effect on urinary function and the quality of life. After one year, 4-6% of the patient population that had brachytherapy reported urine incontinence. Urinary distress symptoms were reported by 11% of the patients one year after radiation therapy. Furthermore, bowel and rectal side effects appear during or shortly after treatment. After one year, 9% of the radiotherapy patients reported urgency, frequency, pain or faecal incontinence. These symptoms were less severe after brachytherapy than after EBRT. Another common side effect is impotence that occurs two or three years after irradiation due to the very late irradiation-induced damage to the neurovascular bundles. Almost 55 out of 100 men have permanent erectile dysfunction in one way or another after radiotherapy. Lastly, fatigue can occur after external irradiation, 4% of the patient feels tired and weak during the weeks of treatment (10).

1.7.5. Experimental surgical and radiological treatment options

Other experimental treatment options are high intensity focal ultrasound (HIFU), cryosurgery and focal therapy. HIFU consists of focussed ultrasound waves on the prostate to induce tissue damage by thermal and mechanical effects. HIFU has shown to have a therapeutic effect in low risk PCa, but further prospective randomised comparison studies are necessary. Cryosurgery uses freezing

techniques to induce cell death. However, unfavourable results are shown for the preservation of sexual function compared to EBRT. Ablating the tumour selectively is very interesting, that is why focal therapy has become an attractive alternative for whole-gland treatment of PCa (36). An additional argument for focal therapy is the fact that local recurrences usually occur at the primary tumour site (37,38). For the implementation of this focal treatment strategy accurate imaging is necessary.

1.7.6. Androgen Deprivation Therapy

Androgen deprivation therapy (ADT) is a hormonal therapy. Androgens play an important role in the development of the prostate and in treatment of PCa. The prostate converts testosterone to dihydrotestosterone, a key substrate for the downstream hormone metabolism. Withdrawal of testosterone by surgical or chemical castration is a well-known treatment for PCa and is effective in 75–80% of patients with metastatic PCa (14). The standard castrate level is <20 ng/dl testosterone level (10). The disadvantage is that there are several side effects associated with ADT: loss of libido, erectile dysfunction, hot flushes, increased bone turnover, significant increased cardiovascular morbidity and fatigue (10).

Different types of hormonal therapy exist. First bilateral surgical castration, which is the best testosterone-lowering therapy, but it is irreversible. Secondly, oestrogens can also lower the testosterone levels without bone loss but this is associated with increased cardiovascular morbidity and mortality. Thirdly, chronic exposure to luteinising-hormone-releasing-hormone (LHRH) agonists results in the down-regulation of LHRH-receptors, suppressing LH and FSH secretion and therefore lowering the testosterone production. Fourth, LHRH antagonists bind immediately and competitively to LHRH receptors in the pituitary gland. This induces a rapid decrease in LH, FSH and testosterone levels. Finally, anti-androgens block the androgen-receptor or can compete with circulating androgens for binding sites on PCa cells. This promotes apoptosis and inhibits cancer cell growth. New ADT drugs are now in phase 3 clinical trials for instance Enzalutamide and Abiraterone (10).

1.7.7. Dr. Therapat project regarding therapy

The patients for this project are recruited from the EC funded project ‘Dr Therapat’. In the Therapat project only patients with low grade prostate cancer are included (T1 –T3a) to identify early biomarkers of PCa. The prostate specimen that is removed by RALP is assessed by a pathologist to determine the TNM stage and Gleason score. This is important to determine the need for further therapy and to decide which therapeutic options are appropriate. The patients can have any additional therapy after the operation because this does not influence the prostate gland itself anymore and therefore has no influence on our study.

1.7. MRI for the detection of prostate cancer

In earlier studies, MRI showed promising results to improve the detection and characterisation of PCa (39–41). By using a multiparametric approach, anatomical and functional information are combined (21). Currently MRI is the only modality that can be used to detect, localise and see the evolution of PCa (37). First, a short explanation will be given about what MRI is in basic steps followed by the role of dynamic contrast enhanced (DCE), T2w MR images and DWI in mpMRI and the function of MRI to follow up treatment of PCa.

1.8.1. MRI in basic steps

MRI uses magnetic fields and radio frequencies to produce images. This imaging system relies on the magnetic properties of hydrogen protons (H^+). When this charged particle is spinning, it produces a magnetic field called a magnetic moment. Normally these H^+ are orientated randomly in the human body so there is no overall magnetic field. However, when an external magnetic field is applied, H^+ align parallel or antiparallel with this primary field (B_0). A greater portion of the protons aligns in the direction parallel to the B_0 , or low energy state. The remaining portion aligns antiparallel to the B_0, called the high energy state. The net result is orientated in the z axis, which points upwards in the direction of B_0 (part *a* on Figure 5). Gradient coils then generate secondary magnetic fields which alter the strength of the B_0 inducing a change of the precession frequencies and phase linearly in the direction of the gradient. These differences in phase and frequencies are the base of the spatial encoding and therefore the reconstruction of the images. Thereafter a radio frequent (RF) pulse is transmitted which flips the H^+ out of the z-axis into the xy plane (plane *b* on Figure 5). On Figure 5 a RF pulse of 90° is used, but other angles are also possible. This RF pulse needs to be of the same frequency (in resonance) as the protons to transfer energy to them. Due to this energy the protons are flipped out of the z axis to the transversal plane and the protons are forced to precess in phase (part *b* on Figure 5). The time that is needed to reassume their normal state is called the relaxation time (plane *c* on Figure 5). There are different types of relaxation: T1, T2 and T2*. Firstly, T1 relaxation is when the sum vector of the protons, that is aligned with the xy plane after the RF pulse, relaxes back to the z axis. T1 relaxation is the time to recover the longitudinal magnetization. The protons can relax because they transfer their energy to the surrounding media, the lattice. Second, T2 relaxation is influenced by spin-spin interactions. The protons in the xy plane split up (dephase) because of energy exchange between individual spins. Due to this proton dephasing, the net magnetization vector in the xy plane becomes smaller. Thirdly, the protons can also precess no longer in phase due to little inhomogeneities in B_0, which is called the T2* effect. These intrinsic inhomogeneities contribute to the dephasing process. T1 and T2 relaxation do not happen independent of each other but simultaneously. The constitution of the tissue determines the relaxation rate. The contrast of the image is determined by the proton density, the T1, T2 and T2* relaxation time of the tissue, and the settings of the MRI namely the echo time (TE), the repetition time (TR) and flip angle (α). The

computer system then receives these signals and performs an analogue to digital conversion. The digital signal, encoded in frequency and phase, is then modified through a Fourier transformation to generate an image encoded in pixel intensity (amplitude).

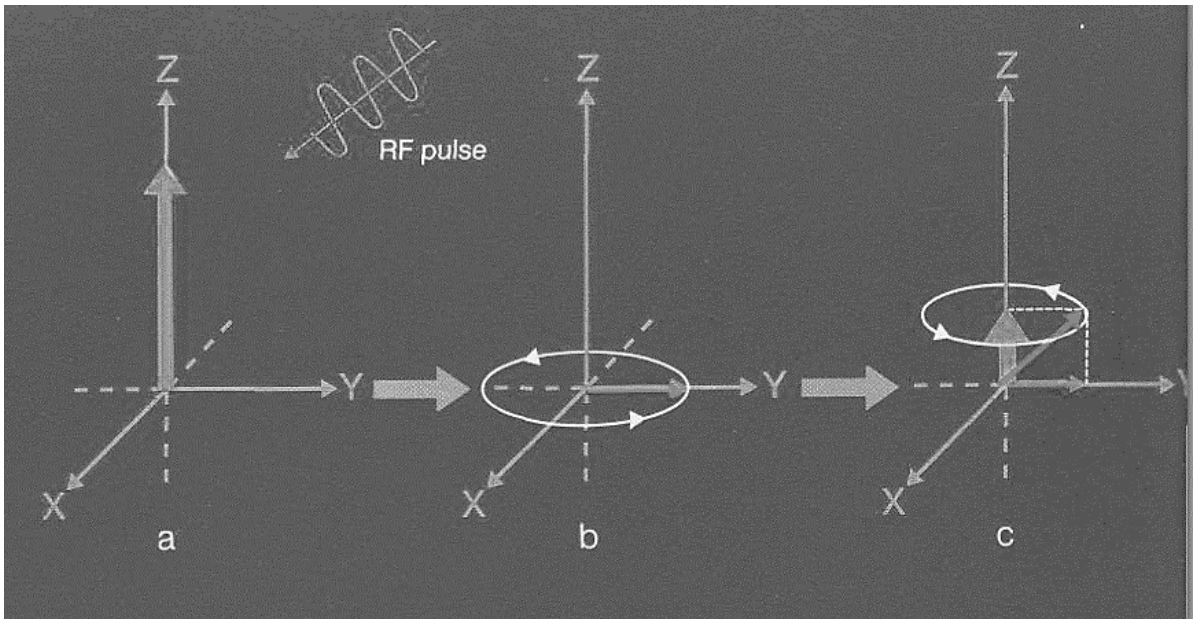

Figure 5. The basic steps of MRI. a) H^+ protons align with the external magnetic field B_0, b) A radiofrequent pulse flips the sum proton vector in the z direction to the xy plane, c) relaxation of the protons back to their original state (a). Figure adapted from (42).

1.8.2. Multiparametric MRI

For the multiparametric evaluation of the prostate, three general MRI sequences are used, namely: DCE, T2w imaging and DWI MRI (36). MpMRI has shown to be able to prospectively visualize PCa tumours with high sensitivity and specificity (5,39,43). As this is the technique that will be used in this study, every MRI sequence will be explained in more detail below.

1.8.2.1. Dynamic contrast enhanced MRI

DCE-MRI uses a T1 shortening contrast agent such as Gadolinium chelates to generate T1 weighted images that characterize tumour biology. Contrast enhanced T1 weighted images have a high sensitivity and specificity for tumour detection. The name T1 weighted images comes from T1 (spin-lattice) relaxation. As mentioned earlier, T1 relaxation is the time to recover the longitudinal magnetization. In DCE MRI, time-dependent changes in T1 relaxatoin due to the distribution of the contrast agent are detected. Gadolinium shortens the T1 relaxation and therefore provides bright signal in images where its concentration is the highest. DCE images visualize the permeability and perfusion properties of tissue. Gadolinium diffuses across the capillary endothelium and characterizes the tumour biology (44). T1 weighted MR images provide anatomical identification of areas of haemorrhage as the high intensity blood signal contrasts with the low signal intensity of the prostate tissue (45). This is especially useful in PCa imaging because TRUS guided biopsies can cause bleedings which can mimic cancer lesions on T2w images. For this reason, a waiting period of six

weeks is recommended between the TRUS guided biopsy and the MRI scan. DCE has high sensitivity and specificity for tumour detection, just as DWI MRI (36). DCE-MRI and DWI provide complementary information about the presence of the tumour, although not always exactly the same tumour locations are pointed out (36). That is why different techniques are combined in mpMRI to overcome the disadvantages of a technique by combining different modalities.

1.8.2.2. T2 weighted MRI

The name T2w images comes from T2 relaxation. As explained earlier, after an RF pulse the protons precess no longer in phase because they get influenced by their neighbours, also called spin-spin relaxation. Mostly fluid appears white on T2w images due to their long T2 relaxation times, in contrast to T1 weighted images where fluid appears dark (42).

Conventional T2w MR images provide anatomical and morphological information about the prostate. That is why T2w imaging is the foundation of mpMRI and is used for radiotherapy treatment planning purposes (30,37). PCa typically presents as a low signal-intensity focus on T2w images. Most of the prostate cancers lesions are located in the PZ which normally displays a high signal intensity due to its high water content (46). This makes it easier to detect the lesions because the contrast is big with the normally high-intensity PZ (6). However, this lower T2 signal can also be caused by haemorrhage, chronic prostatitis, scar tissue, prostate intraepithelial neoplasia, atrophy and posttreatment changes, that resemble cancer (6,46). As mentioned earlier, TRUS guided biopsy, used to diagnose PCa, can cause these haemorrhages. To prevent the problem of haemorrhages that can be mistaken for cancer lesions, there must be at least four to six weeks between the TRUS guided biopsies and the MRI. Additionally, a DCE scan can be performed to identify haemorrhages (6). Tumours in the TZ are more difficult to detect because the normal TZ has already a low T2 intensity. The TZ is also the zone where BPH is located mostly, which can overlap with the cancerous lesions (38). Therefore, the MR images need to be viewed by an experienced radiologist. Furthermore, T2w images are used to evaluate extracapsular invasion, therefore specific criteria for the evaluation of the prostatic capsule, posterior bladder wall and the seminal vesicles can be used (21). Despite the excellent soft tissue contrast, T2w MRI also has several disadvantages, e.g.: tumour volume over- and underestimation, low specificity for lesion characterization and large variation in staging performance (37).

1.8.2.3. Diffusion weighted images

DW MRI measures the diffusion of water mainly within the extracellular space. The diffusion of water is restricted by intra- and extracellular structures and cell walls in the tissue. DWI depends on the net diffusion of water in a specific time period in a specific direction, that is why DWI can reveal both the structure and orientation of tissue, in contrast to T1 and T2 weighted imaging (47). DWI also provides information about tissue cellular density and membrane integrity, adding specificity to the lesion characterisation (21,37). To obtain these images, the normal MRI setting is used, as explained above,

but two diffusion-encoding gradients are added. First, a dephasing gradient is applied that brings the protons out of phase along the gradient direction because the protons are exposed to a different strength of magnetic field, which results in a different precessing frequency of the protons. Thereafter, a second re-phasing gradient is applied in the opposite direction to bring the protons back in phase. The dephasing and re-phasing gradient have exactly the same strength and length and are applied just in the opposite direction making the sum of these gradients zero. However, this only applies to protons that don't move along the direction of the magnetic field gradients, if the protons diffuse they will be exposed to different de- and re-phasing gradients. The sum of these two gradients is not zero anymore, and the protons precess no longer in phase. To conclude, if there is diffusion, the protons precess no longer in phase and the diffusion-weighted signal is lower. DWI is used in mpMRI because in cancerous tissue the cells are more tightly packed than benign cells. Due to the dense tissue, there is less diffusion resulting in a high diffusion signal. Based on these DW images, an ADC map is reconstructed. In each voxel the diffusion constant is replaced by an apparent diffusion constant (ADC) and these ADC maps provide quantitative measures (42,45). Cancerous tissue has a high signal on DW images due to restricted diffusion, but has a low intensity on the calculated ADC maps. DWI has the potential to provide information about the tumour microenvironment and the tumour angiogenesis which gives information about the tumour aggressiveness (48). The disadvantage of DWI images is that a long scanning time is necessary to acquire high spatial resolution images compared to T2w images. Secondly, ADC maps alone are insufficient for accurate delineation of all tumour voxels (48). That is why DWI is complemented with high-resolution T2w images.

1.8.2.4. mpMRI in PCa diagnosis

The criteria for PCa detection on MRI scans, were the following. On T2w images cancer was characterized by a hypo-intense lesion in the peripheral zone or a very pronounced hypo-intense lesion in the transition zone. On DCE images nodular foci with an early, strong enhancement and rapid washout were considered as suspicious, both in the PZ and the TZ. On DWI scans, cancer was recognized as nodular foci with high signal intensity on b1000 and a low signal intensity on the ADC map, both in the TZ as the PZ (37). It has been proven in other studies that there is a moderate negative correlation between the ADC values and the Gleason score, meaning that a higher Gleason score results in lower ADC values indicating a higher grade of PCa (27,38,40). Different studies showed that DWI has the highest sensitivity for tumour localization and tumour volume measurement (49). In the study of Isebaert *et al.*, significantly higher sensitivity values were obtained for the combination of T2w, DCE, and DWI as compared to each modality alone or any combination of two modalities. So combining these three MRI modalities significantly improves PCa localisation (37).

1.8.3. MRI for treatment planning and monitoring

MRI is a non-invasive tool that can visualize the prostate's anatomy and detect tumours. mpMRI has evolved during the last years to the modality with the highest potential to characterize prostate tissue, because it combines the high-resolution anatomic visualisation of T2w images with regional diffusion characteristics by DWI (4). That is why mpMRI is a key imaging modality in planning surgical procedures, evaluation and follow-up (4). mpMRI shows an excellent sensitivity for Gleason score >7 cancers as indicated in (Table 7) (10).

Table 7. Sensitivity of mpMRI in the detection of PCa (%), per Gleason score and tumour volume. Adapted from (10).

Gleason score	*Tumour Volume (ml)*		
	<0.5	**0.5-2.0**	**>2.0**
GS 6	21-29%	43-54%	67-75%
GS 7	63%	82-88%	97%
GS >7	80%	93%	100%

GS= Gleason score

MRI can be used to guide the decision for a particular treatment option, determine tumour aggressiveness, prostate gland evaluation and staging of PCa (21). In low risk patients, the most obvious treatment options are radical prostatectomy or active surveillance. MpMRI can image the lesion accurately which can be helpful in managing low risk patients to guide them towards active surveillance (Table 1). Furthermore, mpMRI can help nerve and continence sparing surgery and can be used for focal radiotherapy (Table 8). Moreover, MRI allows detection of unfavourable prognostic features in active surveillance such as tumour volume and higher grade tumours, particularly in anterior and apical lesions (21). Another benefit of mpMRI is that it can detect anterior tumours that are missed by TRUS guided biopsies. Additionally, biopsies that are targeted by MRI seem to evaluate PCa aggressiveness better than systematic biopsies. However, mpMRI is not recommended for local-staging in low risk patients, because of its low sensitivity for focal extra-prostatic extension (10). In the group of intermediate risk patients, the chance of extra-prostatic spread rises significantly. MpMRI can be used here to detect any spread. In high risk patients, MRI or bone scintigraphy is recommended to detect nodal or skeletal metastases. Using conventional MRI for lymph node staging of PCa is unreliable, as 70% of metastatic lymph nodes in PCa are often small (<8 mm). MRI or CT should be performed if the *a priori* risk of having nodal metastases is >40%, (21). The only disadvantage that is still a concern with mpMRI is the inter-reader variability (10). That is why an experienced radiologist needs to look at the images. In 2013 the European society of urogenital radiology published the prostate imaging reporting and data system (PIRADS). These guidelines were updated in 2015 with the PIRADS version 2 publication. The aim of the PIRADS guidelines is to standardize the reporting of the radiological findings of prostate MRI (50). This standardized system can help to reduce the inter-reader variability and help to implement mpMRI in the standard of care.

Table 8. The role of MRI in different treatment options, adapted from (18).

	Life Expectancy	*AS*	*Radical surgery*	*Radiotherapy*	*Hormones*
Localised	10-15 years	Yes	Yes	External or brachytherapy	No
Localised	<10-15 years	Yes	Rarely	External or bracytherapy	No
Locally advanced	Any	No	Possibly	In combination with hormones	Yes
Metastatic	Any	No	No	Palliative	Yes

AS= Active Surveillance

1.9. 3D printing and histology

In this study, a patient-specific 3D mold is designed based on the *in vivo* MR images of the patients to facilitate the correlation between the MR images and histopathology (5). The 3D printed mold contains a series of evenly spaced parallel slits, each of which corresponds to a known *in vivo* MRI slice, and is used for planning *ex vivo* high-resolution MRI and histopathology (5). The mold serves as a fixative for both the *ex vivo* imaging as for sectioning of the prostate specimen (3,51). The fresh prostate tissue is fixated in the mold to maintain its *in vivo* shape. Thanks to this mold accurate image registration is possible of *ex vivo* MR images with histopathology and *ex vivo* MRI with *in vivo* MRI, because it holds the prostate in the same orientation.

MRI can provide structural information on prostate tissue samples that closely mimics histopathology. Histopathology is the gold standard to evaluate the accuracy of the MR images (52). Tumour probability maps can be correlated and validated with whole-mount histology. The Gleason score and TNM stage are determined based upon histopathological specimens that are H&E stained (37).

1.10. MRI-histology correlation

From literature, it is known that the registration of histology slides to MR images is complicated due to different acquisition artefacts, dissimilar image intensities, shape differences and so on (53). The MRI-histology correlation approaches that are mostly used, can be summarized into three techniques. The first technique relies on sector-based analysis of lesion locations. The second way of registration is the digital mapping of cancer coordinates from one modality to another. The third technique improves tools for gross sectioning. The first approach is limited by the inaccurate knowledge of the true cancer location, while the second approach requires insight in the cutting plane during gross sectioning. The third way can help to control the cutting plane, but does not take morphological changes into account that can occur during the fixation process, e.g. tissue shrinkage (5). In this study, all these approaches will be combined to acquire the best MRI-histopathology correlation. First a pathologist will delineate the lesions on the histopathological slices. Secondly, the 3D mold is used for direct overlay of *in vivo* and *ex vivo* MRI with the histopathological slices. This allows simplification

of the co-registration using the in-house pipeline, which reduces the registration problem from an 3D to a 2D problem. In the in-house-built registration tool, landmarks will be used for correct positioning of the prostate into the mold, additionally to the outflow of the urethra. This registration tool will map the cancer coordinates from the H&E slides to the MR images. Next to the registration tool, the registration will also be performed manually. Out of this histology-MRI registration, the T2 and ADC values of cancerous and non-cancerous tissue will be determined to quantitatively distinguish cancerous lesions from non-cancerous tissue. In the future, this can be used for to identify *in vivo* MRI biomarkers for low grade PCa.

2. Aims of the study

PCa is the most common non-skin cancer in men and the second leading cancer-related cause of death. Therefore, researchers are looking for rapid non-invasive modalities such as MRI to identify PCa patterns for diagnosis and grading. That is why the aim of this project is to identify these patterns by quantitatively distinguish cancerous tissue from non-cancerous tissue. Ideally this could lead to an MRI-based computer assisted diagnosis and grading. In this study the attention is focused on low grade tumors to potentially distinguish between those who require immediate treatment or continues monitoring. In addition, MRI would be a great improvement for the patients compared to the current invasive techniques as TRUS guided biopsies. In this project patients are prospectively included with low grade PCa, T1-T3a, who are scheduled for a RALP procedure. The patients first undergo two *in vivo* MRI scans approximately two weeks before they are operated. These data are used for the generation of patient specific prostate mold. After the prostatectomy, the prostate is fixed in the patient-specific, 3D printed mold and scanned *ex vivo* in a 9.4T MRI unit. Thereafter the fixed prostate is used for pathology where H&E slides are acquired as gold standard. A precise one-to-one correlation between the MRI and histopathology data is possible thanks to the 3D mold. The histology images are registered to the *ex vivo* MR images and this will be correlated to the *in vivo* MR images to allow mapping of the spatial extent of the PCa. The objectives of the project are to validate the reliability of *ex vivo* MRI-based cancer mapping to histology. Based on these *ex vivo* MR scans prognostic and diagnostic markers can be identified. Thanks to MRI biomarkers, more patients can be targeted to active surveillance if imaging could assure good follow-up. This should allow to predict more accurately the disease-specific survival for individual patients, together with a more patient-tailored treatment approach. This study will also look to what extend high-resolution *ex vivo* MRI may guide histopathological exams (5,54,55).

3. Materials and methods

3.1. Workflow of the study

Patients with low grade PCa were recruited for the EC FP7 project 'Dr Therapat' that were scheduled for a RALP procedure. These patients underwent two MRI scans and these images were used for segmentation of the prostate gland and based on these delineations a patient-specific 3D mold was printed. After surgery, the prostate specimen went to Pathology where the tissue was positioned in the mold and fixated. After 24h the prostate was scanned *ex vivo* in a 9.4T MRI scanner with a similar scan protocol as the *in vivo* scanning. The *in vivo, ex vivo* MR images and histopathology slices were all acquired with the same slice thickness and orientation thanks to the 3D mold. Thereafter, the prostate specimen went back to pathology where it was sliced inside the mold. The macroslides generated that way, were then spread out on Plexiglas plates that were scanned with a flatbed scanner at both the front and back. Afterwards, the macroblocks were embedded in paraffin and thin sections of 5 µm were generated with a microtome. Thereafter these slides were H&E stained and scanned. All the images that were acquired in the previous steps were then registered manually and with an in-house designed registration tool.

3.2. Patient population

This study was approved by the local Institutional Review Board and was compliant with the law of experiments on the human being in Belgium of 2004. Written informed consent was obtained from each patient before the first MRI scan. In total fourteen patients were included in the study from January 2014 till December 2015. All patients had biopsy proven, low grade prostate adenocarcinoma and were scheduled for a RALP procedure. Patients that had hormonal therapy or brachytherapy before surgery were excluded. Other exclusion criteria were contraindications for MRI like pacemakers, severe claustrophobia etc. For the Dr. Therapat project, all patients underwent two mpMRI scans containing T2w, DW and DCE scans.

3.3. MRI imaging protocol

3.3.1. In vivo MRI

The patients underwent two mpMRI scans. These scans were performed on a 1.5T MRI unit (Sonata Vision, Siemens, Erlangen, Germany) for patient 1-3 and for patients 3-14 on a 3T MRI unit (Philips Ingenia, Philips Medical Systems, Best, The Netherlands). A combination of a six-channel phased-array body coil and spine coil was used as receiver coils. The *in vivo* MRI scan protocol included a triplanar T2w turbo spin echo MRI scan, an axial DW MRI scan and an axial T1 weighted 3D fast field echo DCE scan with fat saturation. For the DCE MRI scan, an intravenous bolus injection of Gadolinium-DOTA (gadoterate-meglumine, Dotarem, Guerbet, France) was injected at a rate of 2ml/s and a dose of 1ml/15kg. This injection was followed by a 20 ml flush of saline (NaCl 0.9%). For DWI

imaging five b values were used: 0 , 100, 200, 500, 1000 s/mm² and an ADC map was calculated using the following formula $S_n = S_0 \, x \, e^{(-b \, x \, ADC)}$. The imaging parameters that were used during the *in vivo* scan protocol are summarized in Table 9. The orientation of the MR images and the slice spacing was similar to histological sectioning, which was in this case orthogonal to the urethra outflow.

Table 9. *In vivo* imaging parameters summarized.

	TR/TE (msec)	*Slice Thickness (mm)*	*Acquisition Matrix*	*FOV (mm) (FH x RL x AP)*	*Voxel size (mm) (FH x RL x AP)*	*Total scan time (mm)*	*Flip Angle*
T2 weighted TSE axial	2686/95	3	344 x 332	72 x 240 x 105	3 x 0.70 x 0.70	02:30.4	90°
T2 weighted TSE saggital	3476/95	3		240 x 105 x 260	0.70 x 3 x 0.70	03:59.8	90°
T2 weighted TSE coronal	4817/95	3	334 x 336	240 x 240 x 105	0.70 x 0.70 x 3	04:20.1	90°
Axial 3D fast field-echo DCE	4/1.9	3	132 x 129	60 x 260 x 260	3 x 2 x 2	05:06.5	13°
Axial DW spin echo EPI	3500/65	3	116 x 116	66 x 262 x 262	3 x 2.28 x 2.30	03:54.5	90°

TSE= turbo spin echo, DCE= dynamic contrast enhanced, DW= diffusion weighted, EPI= Echo Planar Imaging, TR= repetition time, TE= echo time, FOV= field of view, FH= feet-head, RL= right-left, AP= anterior-posterior.

3.3.2. Ex vivo MRI

After the prostatectomy, the prostate specimen was positioned into the mold and fixated with formalin for at least 24 hours. This mold was then placed in a tubular container filled with formalin and imaged *ex vivo* with a 9.4T Biospec MR scanner (Bruker Biospin, Ettlingen, Germany). The MRI scanner had a bore of 20 cm and a 11.6 cm self-shielded gradient coil was inserted (maximum strength 400 mT/m). The orientation of the prostate specimen was similar to *in vivo* MRI orientation thanks to the 3D mold. This orientation was checked with a Tripilot positioning scan so that the subsequent high-resolution scans could be prescribed accurately. The *ex vivo* MRI protocol included an axial turbo rapid acquisition with refocused echoes sequence (RARE) scan to acquire rapid, low-resolution coronal T2w spin echo sequences, equivalent to the fast spin echo scans acquired on the clinical scanner. Secondly, a fast low angle shot (FLASH) 3D slab coronal scan was acquired followed by a diffusion tensor imaging (DTI) sequence in six directions with a b value of 1500 s/mm². Thereafter two DWI sequences were performed, the first with six directions and three b values, the second with three directions and twelve b values. The final scan was a T2 map with 16 echo times, beginning with 10 ms with and 10 ms echo spacing. The total protocol required maximum 12 hours. The imaging parameters that were used during the *ex vivo* MRI scan protocol are summarized in Table 10.

Table 10. Imaging parameters used during the *ex vivo* scan protocol summarized.

Scan type	*Patients*	*TR/TE (ms)*	*Slice thickness (mm)*	*Matrix*	*FOV (mm)*	*Voxel size (mm)*	*Total scan time*	*Angle*
Tripilotscan 8 cm	All patients	345.18 /5	1	128 x 128	80 x 80	0.31x0.63x1	44s183ms	30°
TurboRARE axial	Pat 1-9	3500/12.55	1	256 x 256	65 x 65	0.25x0.25x1	2m13s0ms	180°
	Pat 10-14	4500/12.55	3	256 x 256	70 x 70	0.27x0.27x3	3m36s0ms	180°
FLASH 3D slab coronal	Pat 1-6	1000/8.1	65	256 x 256 x 256	65 x 65 x 65	0.253x0.25x0.25	39m36s0 ms	20°
	Pat 7-14	150/12	65	360 x 360 x 360	65 x 65 x 65	0.18x0.18x0.18	2h1m30s0 ms	20°
DTI 6dir bval 1500	Pat 1-9	3000/28.68	2.35	64 x 64	65 x 65	1.02x1.02x3	35m12s0 ms	90°
	Pat 10-14	3600/28.68	3	64 x 64	65 x 65	1.09x1.09x3	1h24m28s 800ms	90°
DWI 6dir 3 bval	Pat 12-14	3600/28.68	3.53	64 x 64	70 x 70	1.09x1.09x3.53	1h24m28s 800ms	90°
DWI 3dir 12 bval	Pat 1,3,5-9	2850/28.65	2.35	32 x 32	65 x 65	2.03x2.03x2,35	7h42m4s800ms	90°
	Pat 4,10	2850/28.65	2.35	32 x 32	65 x 65	2.03x2.03x2.35	3h51m2s400ms	90°
	Pat 12-14	3600/28.65	3	32 x 32	70 x 70	2.19x2.19x3	4h51m50s 400ms	90°
T2 map	Pat 1-5	3500/10	1	256 x 256	65 x 65	0.25x0.25x1	33m36s0 ms	180°
	Pat 12-14	4177/10	3	256 x 256	70 x 70	0.27x0.27x3	0h40m6s191ms	143,86°

RARE= rapid acquisition with refocused echoes sequence, FLASH= fast low angle shot, DTI: diffusion tensor imaging, DWI= diffusion weighted imaging, bval= b value, TR= repetition time, TE= echo time, FOV= field of view.

3.4. Segmentation software and 3D printing

To generate the 3D mold the prostate gland was segmented on *in vivo* triplane T2w MRI. The delineation was performed manually by an in-house developed software designed by dr. An Elen with a resolution of 0.469x0.469x3 mm. The prostate was segmented on *in vivo* T2w images that could simultaneously be seen in the three planes: axial, coronal and sagittal. Thanks to the triplane view, an accurate segmentation of the prostate was possible, taking intersecting contours into account. Afterwards the segmentation of the delineated prostate volume was presented separately as a 3D volume that could still be adjusted to the right shape. This delineation was then subtracted from a mold template consisting of a left and right half with predefined cutting slots that exactly matched with the imaging planes. The standard mold had a cylindrical shape with a diameter of 6.4 cm and a length

of 6 cm. A larger mold variant was available to fit larger prostates. Based on this design, a patient-specific mold was 3D printed. The stl-format of the segmentation was uploaded to the 3D printer software UP!. The mold was manufactured from acrylonitrile butadiene styrene (ABS) 1.75 mm 3D printer filament using the UP! Plus 2 3D printer (PP3DP UP!, noDNA GmbH, Berlin, Germany). The printer extruded 0.33 vm^3/min of molten plastic through the hot nozzle. When it arrived on the preheated plate, the plastic cooled down rapidly, printing the mold layer by layer. One half of a mold took approximately 12 hours and was printed with a resolution of 150-400 microns.

The mold contained 14 evenly spaced parallel slits at 3 mm, which corresponded to a known MRI slice *in vivo* and *ex vivo* as well as with the histopathological macroslides. The left and right site was indicated on the mold and the upper, lower, anterior and posterior site were indicated by two L-shaped extensions that were attached to the mold, which resembled the knees of the patient that is lying on his back. After the RALP surgery, the prostate specimen was inked to distinguish the left and right half. Thereafter, the prostate gland was positioned into the mold, enclosed and fixated for 24h in formaldehyde. The mold design was improved after patient six, containing some unique features (Figure 6). By adding the outflow of the urethra and infiltration holes, the prostate was fixated in its *in vivo* shape and possible deformation of the tissue due to fixation was avoided.

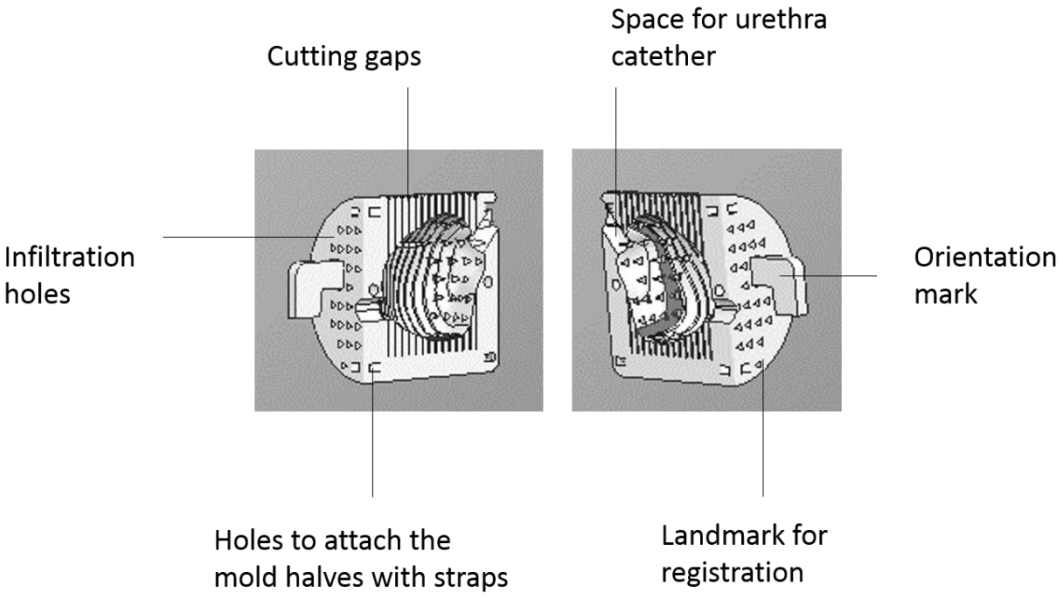

Figure 6. Unique patient-specific 3D printed mold design. Overview of the 3D printed mold design containing: cutting slits at 3 mm, infiltration holes to fixate the specimen inside to mold so that the *in vivo* shape of the prostate is maintained, space for the urethra catheter to reduce mispositioning of the prostate gland, landmarks for registration, an orientation mark to indicate the orientation of the mold and holes to attach the two mold halves with straps.

3.5. Robot assisted laparoscopic prostatectomy

The RALP procedure duplicates the open RRP procedure but with smaller incisions. Five small incisions were made in the lower abdomen and through these incisions the robot-controlled video camera, two assisting instruments and two manipulating wrist-like arms were passed that allow very fine movements. Through the console (Da Vinci) the surgeon manipulated the robot arms while looking with an immersive 3D view to the operative field and was able to direct the camera with hand-controls. The RALP procedure took approximately six hours and was performed by an experienced surgeon.

3.6. Histopathology

The prostate specimen was delivered to the Pathology department where the specimen was first inked to allow proper orientation: blue or red on the right site and black on the left site. When the seminal vesicles were present, these were transected at the base. Thereafter the prostate was weighted and measured left-right, crania-caudal, anterior-posterior. The prostate specimen was placed in the mold with a piece of catheter. The mold was closed with straps and was fixated for at least 24 hours in formalin.

After the *ex vivo* MRI, the prostate was sectioned at intervals of 3 mm perpendicular to the urethra with the mold as fixative. The numbers of slices depended on the total size of the prostate gland. Thereafter, the prostate macroslices of 3 mm were spread out on a Plexiglas plate in order from apex to base and scanned at the front and the back with a flatbed scanner that had a resolution of 0.254x0.254x3 mm. Afterwards these macroslides were paraffin embedded, sectioned in slides of 5 µm with a microtome and H&E stained. These slices were then examined by an experienced uropathologist that outlined all the tumour regions. The pathological tumour stage, the TNM classification (2009), the Gleason score were determined based upon these H&E-stained slices.

3.7. Correlation between MRI and histopathology data

For the registration of the images that were acquired in all the previous steps of the workflow, the *in vivo*, *ex vivo* MRI and histological images, two techniques were used. First, an in-house program was developed to automatically register all the data. Secondly, the histological slides were manually registered to the *ex vivo* MR images. For the second approach, T2 maps, ADC maps and fractional anisotropy (FA) maps were necessary and these were generated manually in ImageJ (version 1.50, National Institutes of Health, Bethesda) and Paravision 5.1 , slice by slice per patient. Signal intensity curves were fitted as a function of the TE (T2 map) or b values (ADC and FA map) with a single exponential decay.

The in house designed registration tool was developed by the following principles. The registration of the H&E slides to the MR images was done in two steps: first the histological slides were registered to the *ex vivo* MR images and then this was correlated to the *in vivo* MRI stacks. So the *ex vivo* MRI was used as intermediate for the registration of the data. The automatic registration tool needed the following data input: for the *ex vivo* MR images; T2w 2D, T2w 3D images and the *ex vivo* ADC map, for the *in vivo* MR images; triplane T2w images and the *in vivo* ADC map. Also the left and right mold file and the segmentation volume were used for the registration, next to the macroslide scans and the H&E slides.

The MR images, both *in* and *ex vivo*, were registered rigidly using maximization of mutual information, assuming that the shrinkage of the tissue was slight. As mentioned earlier, the mold was created based on the triplane *in vivo* MR images. Thanks to the mold, the *ex* and *in vivo* MRI image registration was reduced to matching of the mold shape in both image stacks, because the mold could directly be overlaid on the *in vivo* MR images. Furthermore, a non-rigid 2D registration was used to align the histological slides to the *ex vivo* MR images. This was performed slice by slice based upon a histogram-based similarity measure. The tissue features that were apparent in the tissue on the high-resolution images were used as guidance for the registration. Thanks to the mold all the images that were used, were in the same plane and had the same slice thickness which reduced the registration from 3D to 2D problem.
Secondly, the manual registration, the *ex vivo* MR images were registered to the H&E slides. To be able to do this, the prostate gland was delineated on the *ex vivo* T2w images slice by slice with ImageJ to reconstruct a 3D stack. Thereafter the same was done for the H&E slides, for every patient individually. These two 3D stacks were orientated in the same direction with the T2w slices as reference. Then the T2w and H&E stack were registered rigidly based on mutual information with FSL (version 5.0, University of Oxford, UK). In ImageJ the T2 map, ADC map and FA map were synchronized and the tumour regions, that were delineated by the pathologists, were used as regions of interest. The difference in T2, ADC and FA values of the cancerous lesions were compared with a contralateral healthy regions in ImageJ. This was done for the TZ and PZ separately.

3.8. Statistical analysis

All statistics were tested two-sided, p values <0.05 were considered as statistically significant. Statistical analyses were performed in GraphPad Prism (version 7.00, GraphPad Software Inc., San Diego). First normality of the was tested with Shapiro-Wilk normality test. The difference in T2, ADC and FA values between the cancerous lesion and the healthy contralateral tissue was statistically measured by paired t-tests or the non-parametric equivalent Wilcoxon matched-pairs signed rank test. Thereafter the correlation was tested between the T2 or ADC values and the size of the region of interest (ROI) by the Pearson of non-parametric Spearman correlation coefficient.

4. Results

4.1. Patient characteristics

Fourteen patients with biopsy proven adenocarcinoma were prospectively included in the Dr. Therapat project. These patients had an average age of 68 years ± 6.6 (range from 55 to 77), an average PSA level of 10.46 ng/ml ± 6.7 (range from 2.90 to 24.83 ng/ml) and a median Gleason score was 7 (range from 6 to 8). The clinical characteristics are shown in Table 11**.** All the patients underwent two mpMRI scans. The mean time between the biopsy and the first MRI scan was 117 days ± 184.6 (range from 31 to 727 days). The minimum time needed between the first MRI and the RALP procedure was 2 weeks for logistic reasons and the mean time between the first scan and the surgery was 72 days ± 65.9 (range from 13 to 261 days).

Table 11. Clinical characteristics of 14 patients included in the Dr. Therapat project.

	Pre PSA (ng/ml)	*Age at surgery (years)*	*Gleason score*	*Time between biopsy and first scan (days)*	*Time between first scan and the surgery (days)*
Average	10.45	68	7	117	72
Min	2.90	55	6	31	13
Max	24.83	78	8	727	261

The prostate gland was weighted and measured left-right, crania-caudal, anterior-posterior (Table 12). The H&E slides were examined by an experienced uropathologist and the pathological tumour stage (TNM classification 2009), the Gleason score and tumour volume were determined (Table 12 and Table 13).

Table 12. Prostate gland characteristics of the 14 included patients.

	Prostate volume (cm)	*Tumour volume (total, ml)*	*Tumour volume (% of the prostate)*
Average	4.6 x 4.8 x 4.1	4.75	10.35
Min	3.4 x 3.3 x 3.3	0.1	1.5
Max	5.6 x 6.2 x 5	17.5	30.6

Table 13. Pathological TNM stage and Gleason score with the number of included patients per condition.

		Number of patients
TNM stage	2a	1
	2c	7
	2c+	1
	3a	5
Nodule invasion	Nx	8
	N0	5
	N1	1
Gleason score	3+3	4
	3+4	9
	4+3	3
	4+4	1
Location of the tumour	TZ	2
	PZ	15
	Base	3
	Left	3
	Right	3
	Left and Right	5

4.2. Registration of all the acquired images

The registration of the histology to the MRI data was performed manually and with the registration tool.

4.2.1. Manual registration

The ADC values were pooled for the seven patients that fit in the mold. For the last patient included in the study, the H&E slides were not processed by the deadline of the thesis. One patient was excluded due to ghosting of the *ex vivo* MR images and another patient was excluded due to too little tumour lesions delineated by the pathologist. The tumour volume of this last patient was 1.6% of the total prostate volume. So the results that were obtained, are based on the seven remainder patients. The T2 values were calculated for four patients of these seven patients where a T2 map was acquired *ex vivo*. FA maps were calculated for the same four patients.

4.2.1.1. Comparison of T2 and ADC values between healthy and cancerous tissue

T2 and ADC values of healthy and cancerous tissue were compared in the TZ and PZ separately. The average T2 values of the TZ were: 0.05281±0.0199 sec for the healthy tissue and 0.0505 ±0.01839 sec for the cancerous lesions. When these were compared to each other, no significant difference was shown (p=0.1522, Wilcoxon matched-pairs signed rank test). The same was done for the T2 values of the PZ. The average T2 values for healthy tissue were 0.05265 ±0.02818 sec and 0.04806 ±0.02369 sec for cancerous lesions. When these were again compared to each other, also here no significant difference was found (p=0.2492, paired t-test).

The average ADC values of the TZ were 0.6106±0.15140 mm²/sec for healthy tissue and 0.4485±0.117 mm²/sec for cancerous tissue. The ADC values of the TZ of healthy and cancerous tissue were significantly different (p<0.0001, Wilcoxon matched-pairs signed rank test). For the ADC values of the PZ, the average ADC values for healthy tissue were 0.5404 ±0.1316 mm²/sec and for cancerous lesions 0.4979±0.08491 mm²/sec. The reciprocal difference was not significant (p=0.0904, paired t-test). All these results are represented in Figure 7.

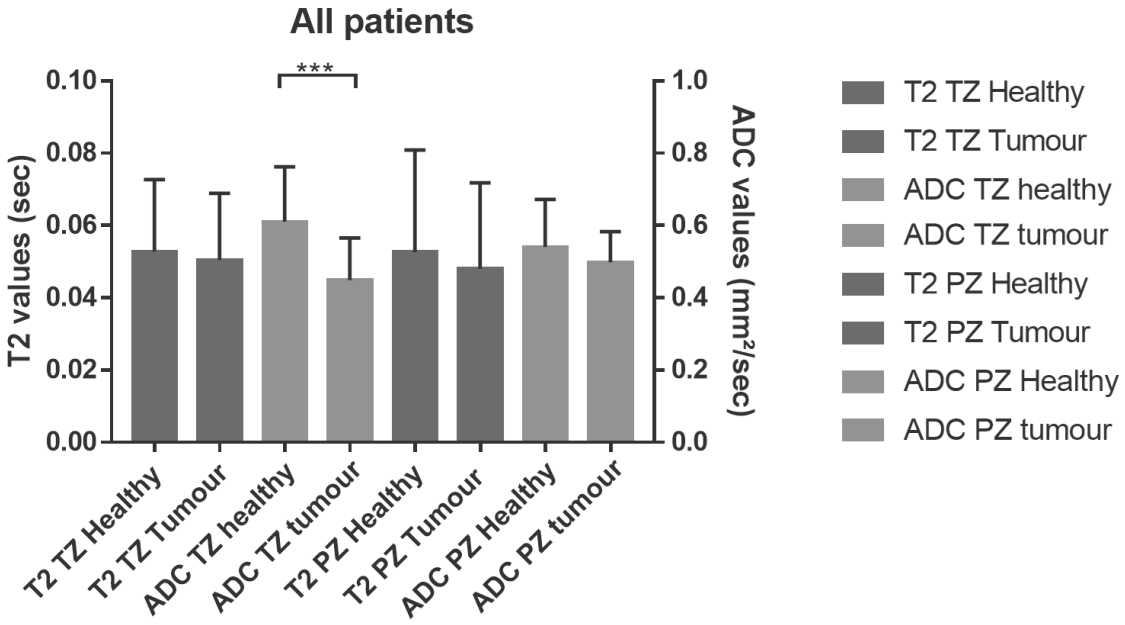

Figure 7. Comparison of T2 and ADC values between healthy and cancerous tissue. Difference between the T2 or ADC values of the PZ and TZ statistically tested with paired t-tests or Wilcoxon matched-pairs signed rank test as non-parametric equivalent. Significant difference was found between the healthy and cancerous ADC values in the TZ (p<0.0001). TZ= transition zone, PZ: peripheral zone, ADC= apparent diffusion coefficient.

4.2.1.2. Biomarker for cancerous tissue on MR images

In the scatterplot on Figure 8, three groups can be distinguished in the T2 values of healthy tissue in the PZ. These three groups correspond to three different patient groups: the lowest values are from patient 3 and 5, the highest values were obtained from patient 4. The same groups come back in the T2 values of cancerous tissue in the PZ where 2 distinct groups can be distinguished, the lowest values correspond to patient 3 and 5 again, the highest group values come from patient 4 and 12. Similar group formation can be observed in the T2 values in the TZ. In healthy tissue, three groups can be distinguished: the lowest group corresponds to patient 5, the middle group to patient 12 and the highest values to patient 4. In the cancerous lesions, again three distinct groups can be observed form the same patients: the lowest values correspond to patient 5, the middle group to patient 12 and the highest values to patient 4. If this trend of group formation in T2 values is compared between the TZ and the PZ, than there can be concluded that the lowest values were measured in the MR images of patient 5, the middle group corresponds to patient 12 and the highest values were measured in the images of patient 4. Kruskal-Wallis tests were performed to see if the difference in T2 values was

significant between patients. They were corrected for multiple testing with Bonferroni correction which brought the significance level to p<0.0125. The difference in T2 values between patients was significant for the PZ for healthy and cancerous T2 values (Healthy: p= 0.0005, Cancer: p=0.0002). This was similar for the TZ, where a significant difference between the samples was shown for the healthy and cancerous T2 values (Healthy: p=0.0008, Cancer: p=0.0006). No distinct groups were formed in the ADC values, neither in the TZ nor in the PZ.

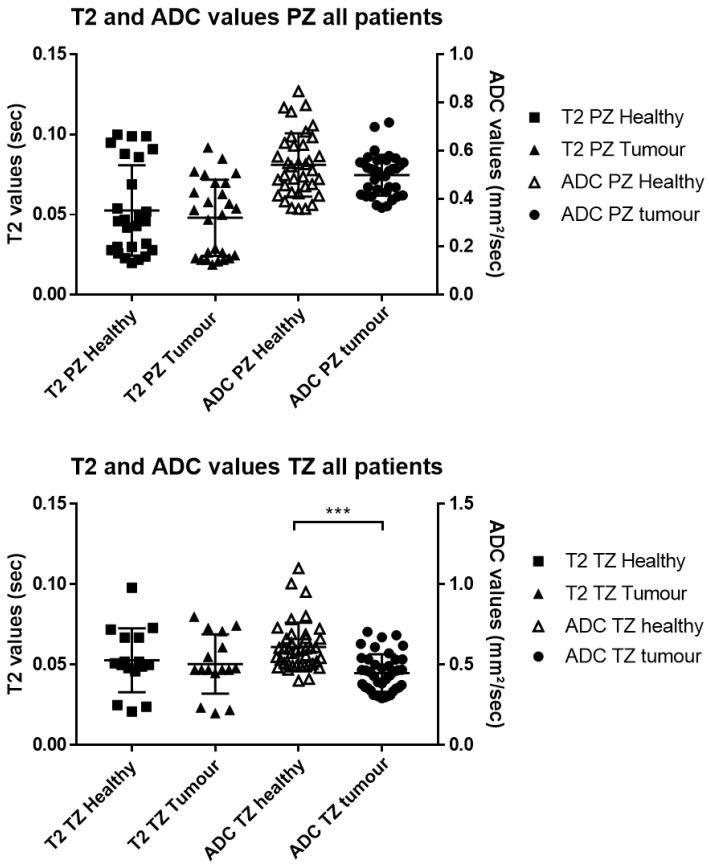

0

Figure 8. Scatterplot of the T2 and ADC values of all patients. A trend can be observed that distinct groups are formed in the T2 values of healthy as well as the tumour lesions of the TZ and PZ. These groups correspond to different patients. Patient 3 and 5 have the lowest T2 values in both healthy and cancerous regions. This is true for the TZ as well as the PZ. Patient 12 corresponds to the middle values and the highest T2 values were measured in Patient 4. No group formation was observed in the ADC values. TZ= transition zone, PZ= peripheral zone, ADC= apparent diffusion coefficient.

4.2.1.3. Possible correlation of T2 or ADC values and tumour size

The next question was to see if there was a correlation between the T2 or ADC values and the size of the tumour. Therefore, the T2 and ADC values were correlated with the size of the ROI for the TZ and PZ separately. Here a correlation was seen between the area size and the T2 values in the healthy PZ zone (p=0.0003), the T2 values of the cancerous PZ values (p=0.0014) and the T2 values of the healthy TZ zone (p=0.0086). There was however no correlation between the T2 values of the cancerous TZ zone and the size of the ROI (p=0.2561). Similar results were found for the ADC maps where there was a correlation with the tumour area and the cancerous ADC values in the PZ

(p=0.0122) and in the TZ (p=0.0006). In the healthy PZ and TZ, there were no significant differences found between the ADC values and the size of the ROI (PZ: p=0.9513, TZ: p=0.8767) (Figure 9).

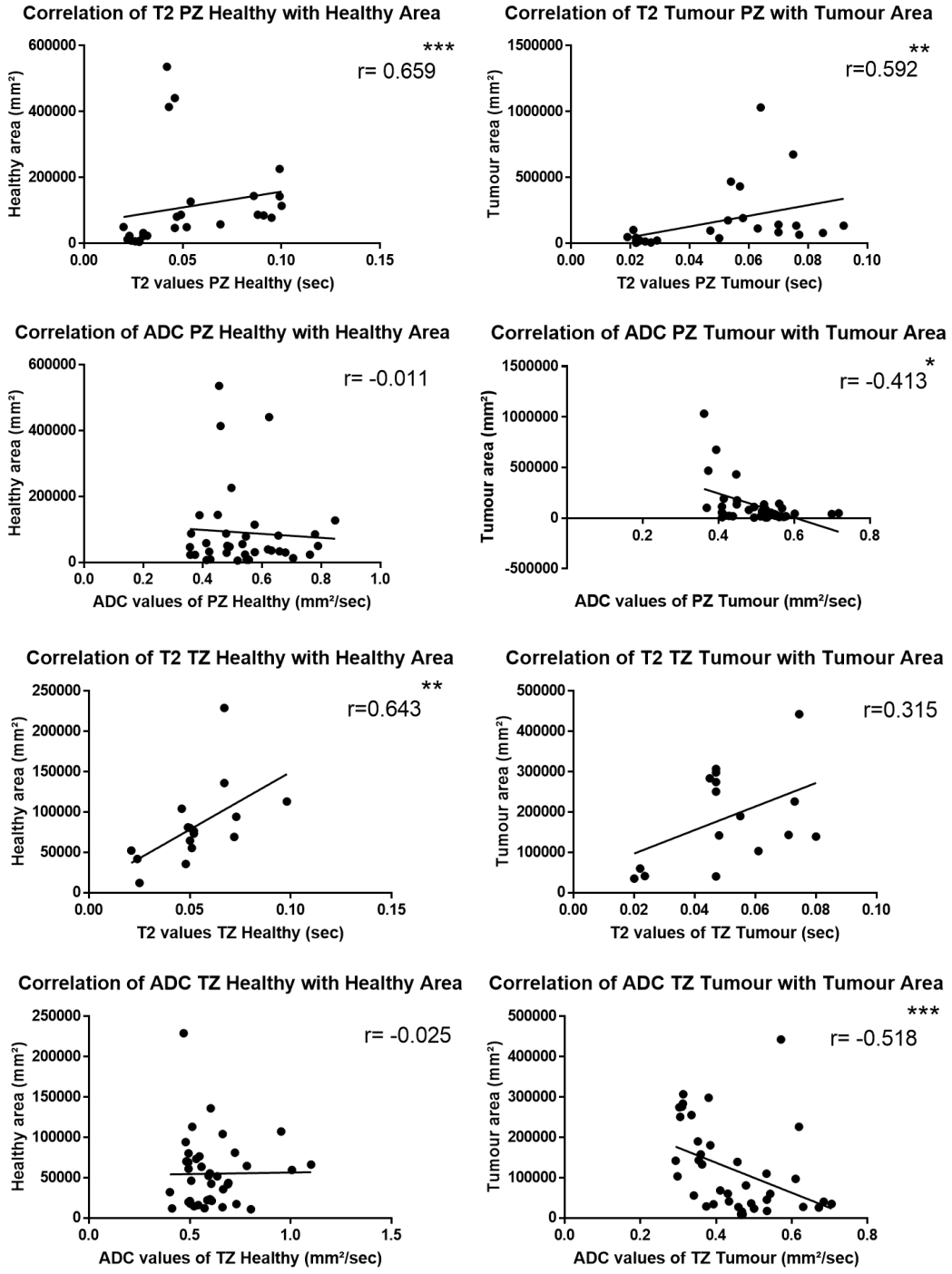

Figure 9. Correlation between T2 and ADC values with tumour size. For the PZ, a significant correlation was found between the T2 values and the healthy area (p=0.0003), the T2 values of the tumour region and the tumour area (p=0.0014), the cancerous ADC values and the tumour size (p=0.0122). No significant correlation was found between the healthy ADC values and the size of the area in the healthy PZ (p=0.9513). For the TZ similar results were obtained. A significant correlation was found between the healthy T2 values and the healthy area (p=0.0086), and the cancerous ADC values and the tumour area (p=0.0006). No significant correlation was found between the cancerous T2 values and the tumour area (p=0.2561), and the healthy ADC values and the healthy area (p=0.8767) in the TZ. TZ= transition zone, PZ= peripheral zone, ADC= apparent diffusion coefficient.

4.2.1.4. Fractional anisotropy as biomarker

The *ex vivo* FA values from healthy tissue were compared with cancerous lesions in the TZ and PZ separately. This was done by Wilcoxon matched-pairs signed rank tests and Bonferroni correction was applied to correct for multiple testing, which reduced the significance level from $p<0.05$ to $p<0.0125$. Significant differences were observed between healthy and cancerous tissue in the TZ ($p=0.0004$). In contrast to the PZ where no significant result was shown ($p=0.2877$). The FA values from the TZ and PZ were also compared to each other and no significant differences were obtained, not in the healthy tissue ($p=0.3926$) nor in tumour lesions ($p=0.5168$) (Figure 10).

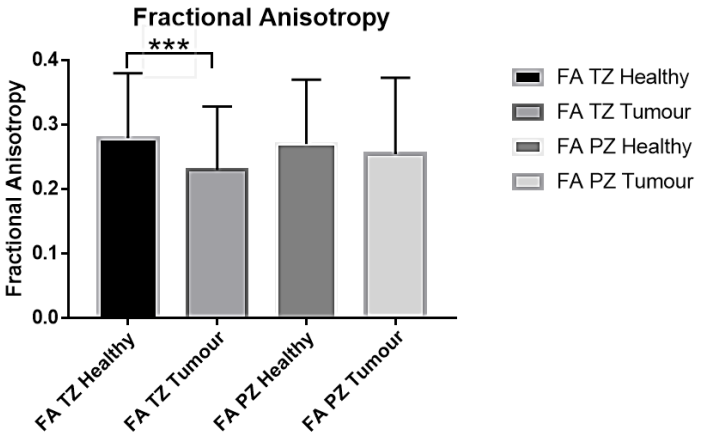

Figure 10: Fractional anisotropy between healthy and cancerous tissue in the transition zone and peripheral zone. A significant difference was obtained between FA from healthy and cancerous tissue in the TZ ($p=0.0004$). In contrary to the PZ where no significant difference was shown ($p=0.2877$). The FA values were also tested between the TZ and PZ. Here no significant difference was obtained for both healthy ($p:0.3926$) and cancerous tissue ($p:0.5168$). FA= fractional anisotropy, TZ= transition zone, PZ= peripheral zone.

4.2.2. Registration tool

The registration tool was an in-house designed module in Mevislab (version 2.3.1. , MeVis Medical Solutions AG, Bremen, Germany) that registered the H&E slides to the *in vivo* MR images, with the *ex vivo* MR images as intermediate. To make the registration of the images easy and robust, it is based on a limited degrees of freedom. In this tool, eight steps needed to be performed.

4.2.2.1. 3D macroblock reconstruction

The first step of the registration tool was a 3D reconstruction of the prostate based on the 3 mm macroblock slides that were scanned with a flatbed scanner. These macroblocks were generated when the prostate was sectioned via the slits of the mold. As the macroslides were scanned at both sides, the prostate gland could be reconstructed. For every patient two plates with macroblocks were scanned. In a first step, these two plates were orientated in the same direction, the background was indicated and the order of the slides was selected from apex to base. Thereafter the inside of each macroslide and the background were indicated. Finally the macroslide with the least overhanging edges was selected to make a 3D reconstruction of the macroblocks of the prostate. The workflow of this tab is shown in Figure 11.

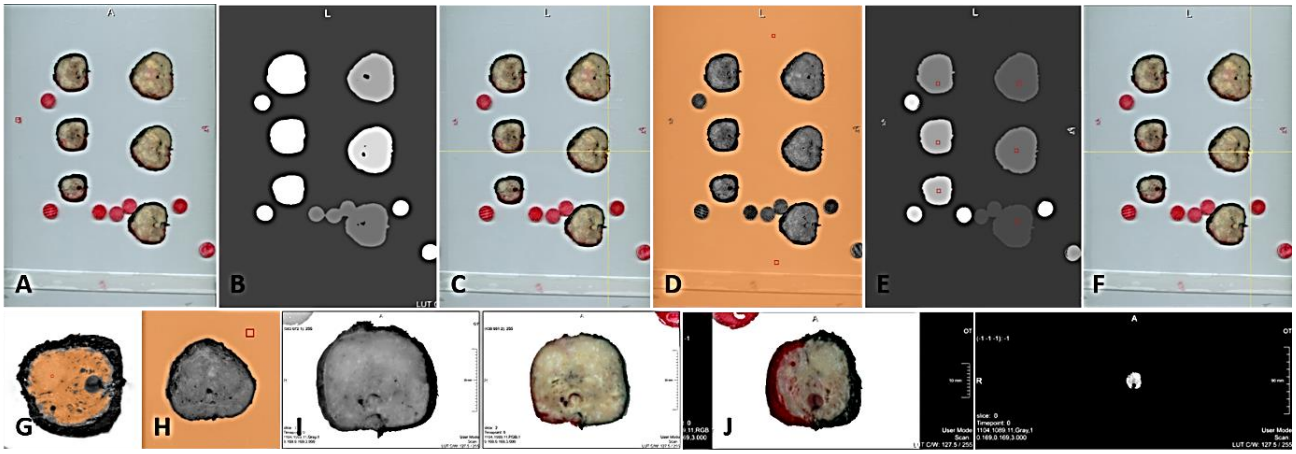

Figure 11. 3D macroblock reconstruction with the registration tool. Orienting the scans of the macroslides in the same direction (A) and indicating the background of the plate (B). The registration of this step needed to be checked by controlling registration for landmarks (C). The background of the plate was indicated (D) and the macroslides were selected from apex to base (E) for which the registration also needed to be confirmed a second time (F). Thereafter the inside of each macroslides (G) and the outside (H) was selected. In the last step the slide with the least overhanging edges was chosen (I) to get the 3D macroblock reconstruction (J).

4.2.2.2. Ex vivo to in vivo T2w image registration

The second step connected the *ex vivo* T2w images to the *in vivo* T2w images. In this step the front and the back of the image stack needed to be indicated before the *in* and *ex vivo* images could be manually connected as shown in Figure 12. The connection of the stacks was based on shape. When this registration step was successfully done, this transformation was also applied on the *ex vivo* 3D T2w images and the *ex vivo* ADC map.

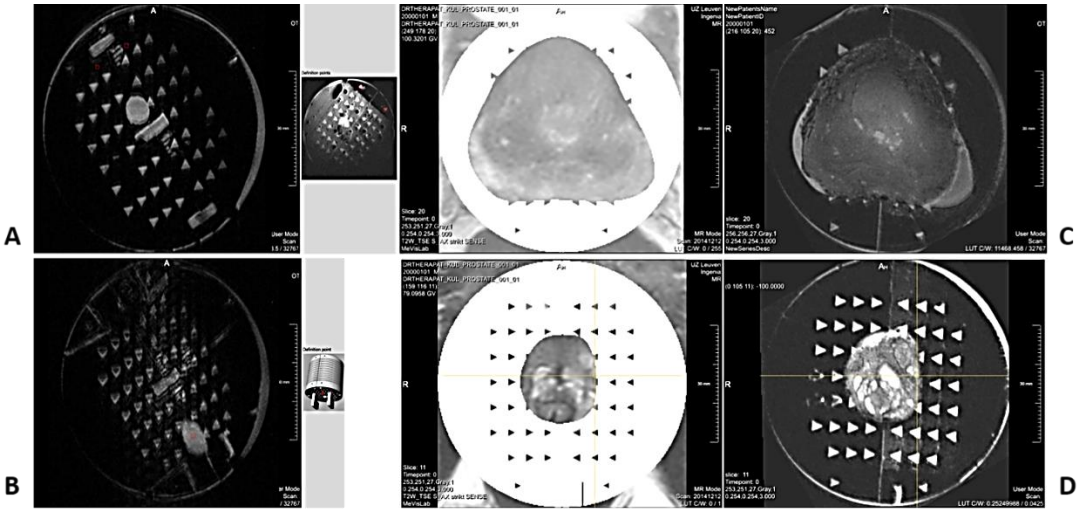

Figure 12. The second step of the registration tool connected the *ex vivo* T2w images to the *in vivo* T2w images based on shape. First the front (A) and the back (B) of the *ex vivo* T2w stack needed to be indicated. Thereafter the *in vivo* MR image stack was connected with the *ex vivo* T2w stack based on shape (C), and this results was then checked with landmark registration.

4.2.2.3. Check mold positioning

The third tab in the registration tool was to check the positioning of the mold on the *in vivo* MR images to check if the prostate tissue was correctly positioned in the mold or not. Manually landmarks were indicated to register the images and then the resulting rotation around every axis was reported (Figure 13).

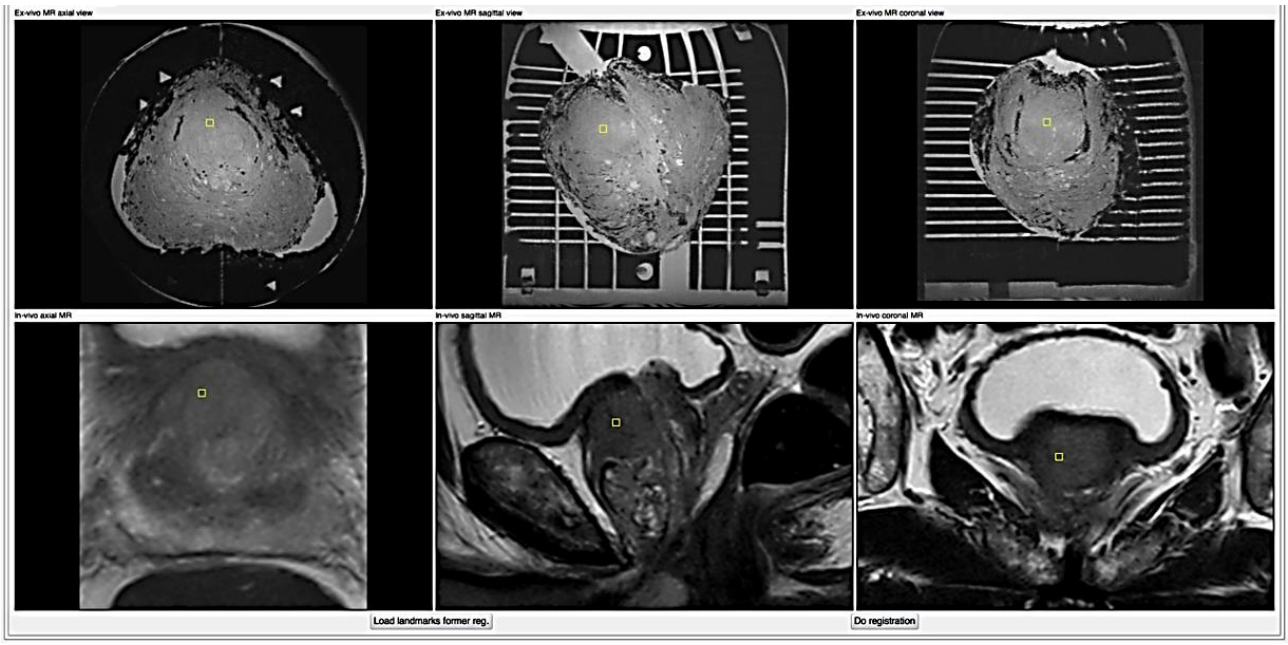

Figure 13.Check mold positioning as third step in the registration tool. Third tab of the registration tool: checking the mold position to see if the prostate specimen was correctly positioned into the mold. The resulting rotation around every axis was then reported.

4.2.2.4. Macroblock to in vivo MR image registration

The fourth step of the registration tool (MB 2 in) registered the 3D macroblock stack formed in step 1 to the *in vivo* MR images. This registration was based on the patient-specific 3D mold. The corresponding macroblock needed to be connected to the matching *in vivo* MR image (plane *A* Figure 14). This was based on the indications of the pathologist on the cutting template paper. This was a form where the pathologist indicated where the first cut was done, relative to the mold (plane *C* Figure 14). If the registration was not properly done, this could be adapted manually. This result was checked again by landmark registration (plane *B* Figure 14).

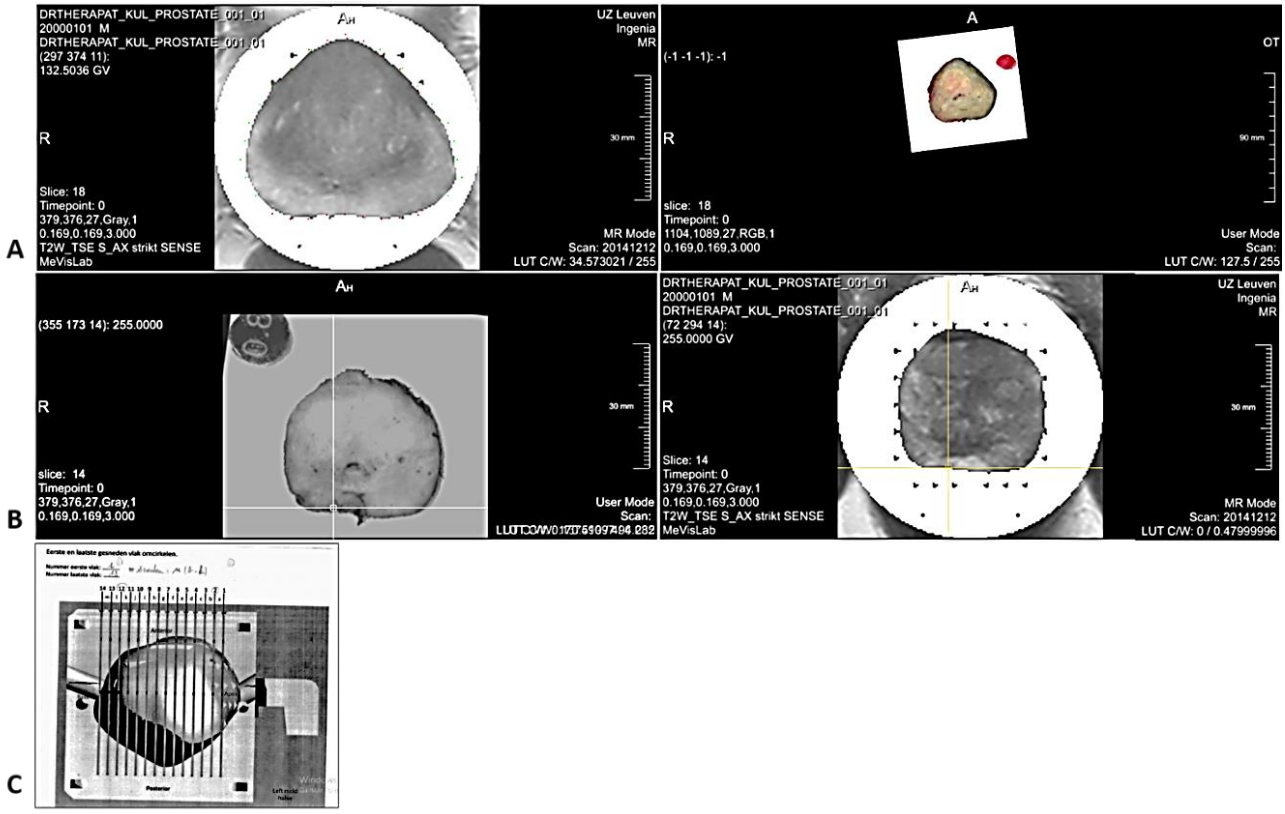

Figure 14. Fourth step, 3D macroblock stack registered to *in vivo* MR images. In the fourth step of the registration, 3D macroblock reconstruction was registered to the *in vivo* MR images (A). The macroblock stack, made in step 1, was connected to the *in vivo* MR stack based on the cutting template (C). This result was again checked based on landmarks (B).

4.2.2.5. Tumour segmentation

The tumour lesions were traced on the histology slices in the fifth step of the registration (Figure 15). Here no registration was performed, but the traced tumour regions were used for the next step of the registration tool where the tumour segmentations were transformed together with the histology images.

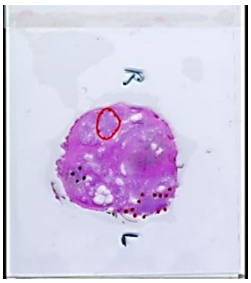

Figure 15. Tumour segmentation. In the fifth step of the registration, the tumour lesions were traced based on the pathological delineations on the H&E slides.

4.2.2.6. Histology to ex vivo MR images and macroblock stack registration

The sixth step of the registration (the Hist 2 Ex/MB tab) registered the histology images to the *ex vivo* MR images and the macroblock stacks. The tumour segmentations that were traced in the previous step, were transformed here. In the first step the most apical macroslide (plane *A* Figure 16) and the inside of the mold was selected by clicking in every slide where tissue was present (plane *B* Figure 16). Then the empty gaps in the mold were coloured (plane *C* Figure 16). These gaps were present when the prostate specimen was a bit smaller than the designed 3D mold. Thereafter the histology slices were initialized by indicating the right and anterior of every H&E slide and indicating a region of interest (plane *D* Figure 16). In this step the *ex vivo* MR and macroblock images were shown as a reference to indicate right and anterior. If the registration was not done accurately, this could be adapted manually by indicating at least three corresponding points per slice. The transfer of the tumour segmentations from the previous tab onto the T2w *ex vivo* images and the macroslides was checked in the last step of this tab (plane *E* Figure 16).

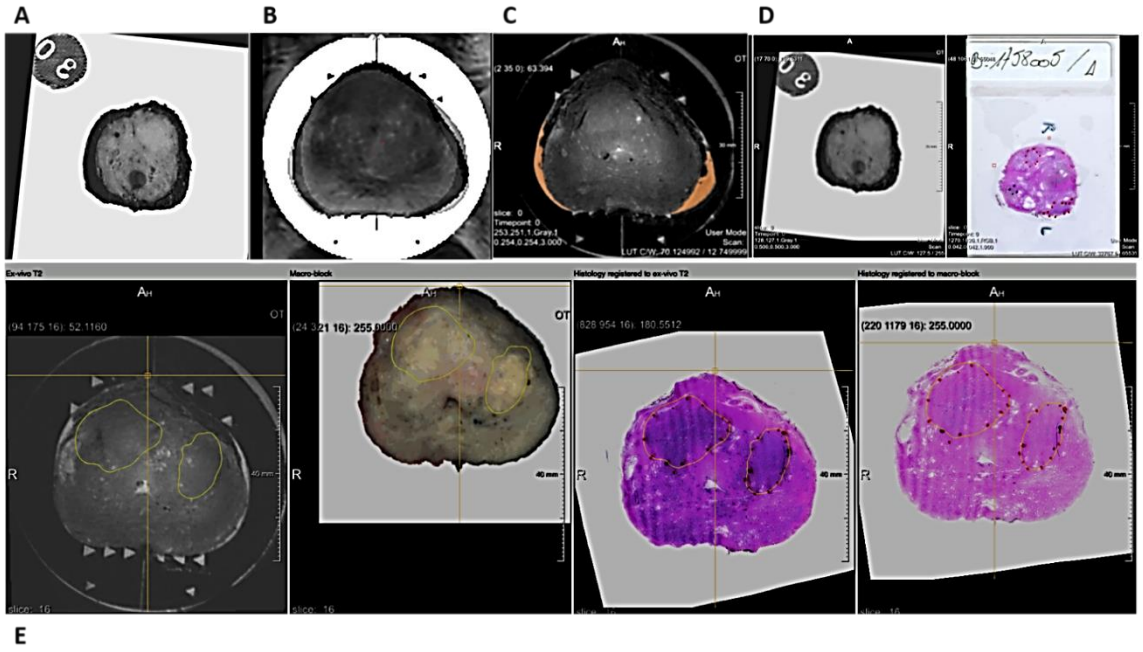

Figure 16. Step six of the registration tool registered the histology images to the *ex vivo* MR and macroblock stack. Indicating the most apical macroblock slide (A) and the tissue inside the mold (B). Then the empty gaps in the mold were coloured (C). Thereafter the histology slides were initialized manually by indicating the right, anterior and a region of interest (D). The transfer of the tumour regions onto the T2w *ex vivo* images and the macroslides was checked in the last step of this tab (E).

4.2.2.7. Functional images

The last tab of the registration was called functional images and transformed the *in vivo* ADC map to match it to the *in vivo* T2w MR images. The same was done for the *ex vivo* ADC map that was registered to the *ex vivo* T2w MR images. The transformation of the *ex vivo* ADC map was already done in step 2, here only the result was loaded (Figure 17). The images were calculated automatically based on the mold that was used to define the ROI in the fourth tab.

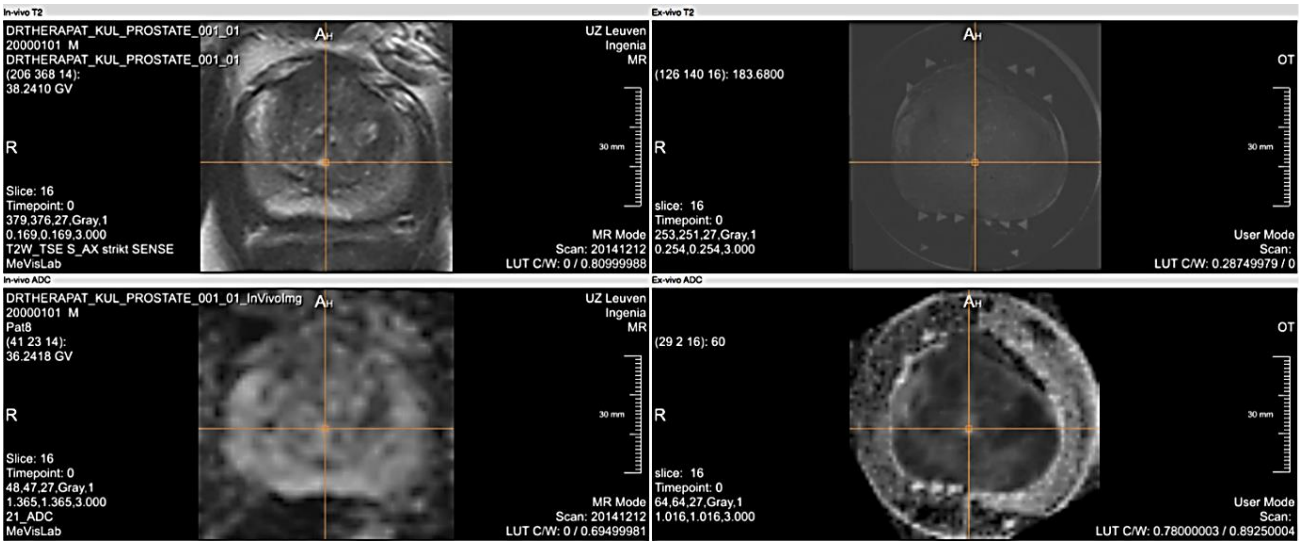

Figure 17. The last registration tab, functional images. The last registration tab, functional images, transformed the *in* and *ex vivo* ADC maps to match them to the *ex vivo* T2w MR and the *in vivo* T2w MR images that was cut out the mold.

4.2.2.8. Results of the coregistration

In the tab 'Results' an overview was given of all the registered images from the previous steps together with the delineated tumour segmentations (yellow on Figure 18). The registration tool correctly registered the tumour delineations on all the images (Figure 18).

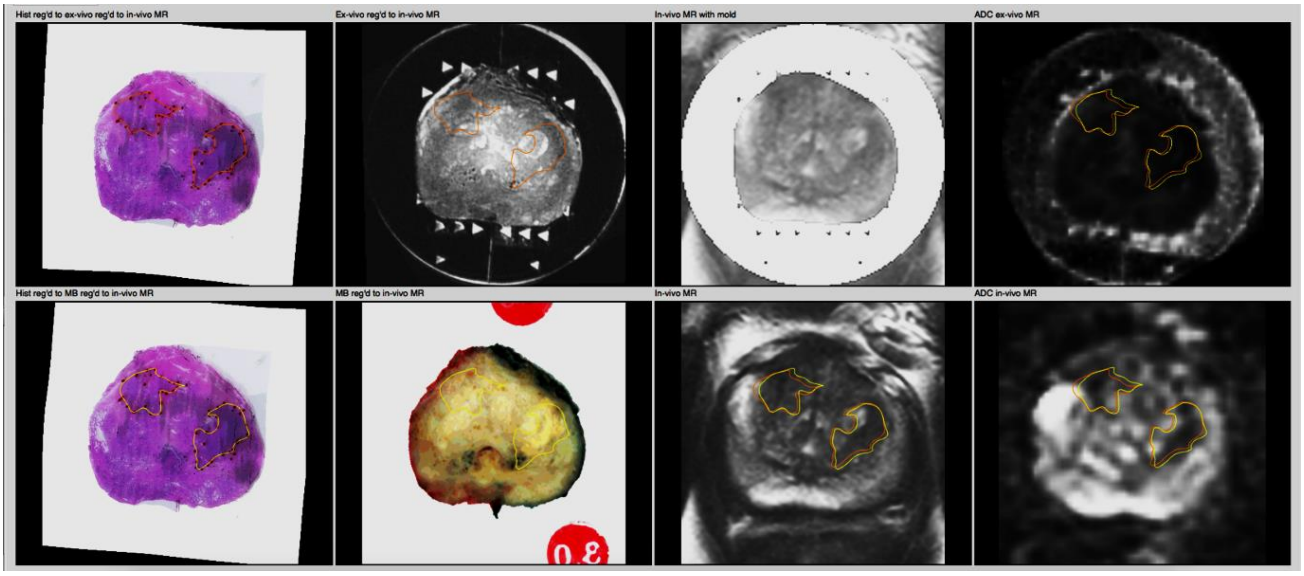

Figure 18. Overview of the results as last step of the registration tool. In the tab 'Results' an overview was given of all the registered images with the tumour segmentations. Legend of the individual images in the top row from left to right: Histology slide registered to *ex vivo* MR and to *in vivo* MR, *Ex vivo* MR stack registered to *in vivo* MR, *in vivo* MR data with the mold, *ex vivo* ADC map. Bottom row from left to right: histology slide registered to the corresponding macroblock image and registered to *in vivo* MR data, macroblock image registered to *in vivo* MR, *in vivo* MR stack and *in vivo* ADC map.

5. Discussion and conclusion

5.1. Aim of the project and patient selection

PCa is the second leading cause of cancer death in men (56). Due to this serious topic, current research is focused on non-invasive techniques for diagnosing and grading PCa. Now the standard of care diagnosis of PCa this is still based on invasive techniques as TRUS guided biopsies (10). mpMRI is a very promising non-invasive modality that is increasingly used in clinical practice in different application including: tumour detection, planning of biopsies, treatment selection, surgical planning, monitoring of active surveillance and radiological therapy planning (55,57,58). During the latest years, disease-targeted therapies emerged and therefore accurate imaging of the tumour localization is very important. Thanks to mpMRI, treatment management can increasingly tend to active surveillance or focal therapy which improves the quality of life for the patients and reduces the financial burden in the future (3). Due to the increased use of TRUS-biopsies the last decade, more clinically indolent tumours are detected which poses an ethical, clinical and financial dilemma.

In this study, patients with low grade biopsy proven adenocarcinoma were included. Low grade patients have the potential choice for active surveillance or to go for RALP surgery. It is important that they are guided in this decision and mpMRI could give a possibility for intensive follow-up by imaging. Unfortunately, low grade tumours have less vascular density than high grade tumours and that is why their detection on DCE MR images is more difficult (59). Therefore, more research is necessary on low grade tumours to determine imaging biomarkers in low grade tumour mpMRI scans. In this study, patients underwent two mpMRI scans voluntarily for validation of the imaging protocol (60). Now the clinical protocol for prostatic mpMRI scans will be adapted so that all the patients that had a prostatic mpMRI scan could be included in the study. The only step that will be different than from the clinical procedure will be the *ex vivo* scanning of the prostate after the surgery. Future patients will undergo a streamlined and shortened *in vivo* imaging protocol, which will improve patient recruitment and clinical implementation.

5.2. Obstacles of mpMRI validation and implementation in clinical practice

Now mpMRI still needs to be validated by histopathology as histology is the gold standard for cancer characterization. In this project, the aim was to cross-link information provided by *in vivo* mpMRI, with cellular information to identify potential biomarkers to be able to detect the extent and aggressiveness of low grade PCa on *in vivo* MRI (3,59,60).

Hereby, high-resolution, high-field *ex vivo* MRI was used to link the *in vivo* imaging data with histology. The major obstacle for current validation approaches of mpMRI is the lack of accurate registration of MR images with histological data. Different registration systems are used in literature. First, lesion-based comparison, although this is especially difficult in low grade PCa, as low grade PCa is heterogeneous and multifocal (59). Secondly, sector-based comparison where the prostate gland is divided in six sectors resembling pathological examination but this is based on many assumptions (59). Thirdly, 2D MRI slide registration to the corresponding H&E slide, which is very time consuming and labour intensive (61). Fourthly, the registration of a 3D histology volume with the 3D MRI volume, but the two last methods do not take prostate deformation into account (58).

5.2.1. Prostate deformation

As these different techniques all have their disadvantages, research focuses on a method for automatic registration. However, this is not easy due to differences in image intensities, acquisition artefacts and shape (58). The prostate gland that is imaged *in vivo* is not the same as the *ex vivo* prostate due to prostate deformation. This prostate deformation is caused by various influences (58). First of all the shape of the prostate gland is influenced by filling of the rectum and bladder (62). If endorectal coils are used, the prostate shape is even more changed. These endorectal coils could compress and deform the prostate, confounding the comparison with the *ex vivo* prostate. In the study of Heijminck *et al.* a 18% difference in prostate volume was measured on MRI with or without endorectal coil (4). Therefore, in our study no endorectal coils were used to avoid prostate compression and for the patient's comfort. Secondly, the surgical procedure itself also influences the prostate tissue. During surgical extraction, the vascular and urethral pressure fall away, there is manual compression by the surgeon and tissue destruction which results in a 10% loss in volume of the prostate gland (58). In the study of Orckzyck *et al.,* the prostate volume was significantly smaller *ex vivo* than *in vivo*, with a 19.5% difference. The three imaging planes were investigated but only in the axial plane the prostate gland was 12.2% larger *ex vivo* than *in vivo*, which suggest that the size reduction was not homogenous between the three dimensions (57).

The third influencing factor on prostate deformation is the fixation process. Fixation and paraffin embedding induce dehydration of the tissue, which causes shrinkage of the internal tissue. The cutting process to obtain 5 µm histological sections could also induce non-uniform cutting deformation. Next to these three *ex vivo* prostate deformations, the prostate gland also moves during *in vivo* imaging. Due to breathing, the prostate gland moves with a difference of 1 cm between full inspiration and expiration. Although, in comfortable position this motion is reduced to 4 mm (58). Therefore, the *in vivo* MRI should be respiratory gated. As there are different types of prostate deformation, *in vivo* as well as *ex vivo*, this should be taken into account during the registration of histological data to *in vivo* MR images.

5.2.2. Biomakers for low grade prostate cancer determined by *ex vivo* MR imaging

5.2.2.1. Comparison of T2 and ADC values between healthy and cancerous tissue

T2 and ADC values were compared between healthy and cancerous tissue in the TZ and PZ. The ADC values of cancerous tissue were significantly lower than those of healthy tissue in the TZ ($p<0.0001$) (Figure 7). These lower ADC values are consistent with literature where a significant difference was observed between healthy and cancerous tissue *in vivo* as well as *ex vivo* (63,64). These lower ADC values in cancer tissue indicate reduced water mobility in tumours and increased cell density (65).

The ADC values of cancerous tissue were also compared between the *in vivo* and *ex vivo* registration data. The ADC values *in vivo* were 2.21 times higher than *ex vivo*. This difference in ADC values could be attributed to fixation of the tissue. This same decrease was observed in the study of Bourne *et al.* (65). In the study of McGrath *et al.,* the decrease in T1, T2 and ADC values *ex vivo* compared to *in vivo* was attributed to fixation of the tissue. T2 and ADC values decreased particularly at the edge of the tissue whereas the T1 values decreased uniformly (66). Biomedical properties of the prostate tissue change during fixation and these fixation effects can change with the distance from the edge, variation in tissue type and the orientation during fixation (67). Formalin-fixed prostate tissue can create or exaggerate a diffusion difference that is not present in fresh prostate tissue and this suggests further investigation (47).

5.2.2.2. Group formation per patients in T2 values on the scatterplot

Out of the scatterplot on Figure 8, could be concluded that there was group formation in the T2 values between healthy and cancerous tissue, both in the TZ as the PZ. The patient-related difference was significant in T2 values of the TZ as well as in the PZ. This inter-individual difference in T2 values could not be explained by histology, but it was noticed that the fixation time varied slightly. Patients 3 and 5 had the lowest T2 values and both prostates were fixed for 2 days. The prostate gland of patient 12, who had intermediate T2 values, was fixed for 1 day. Patient's 4 prostate, who had the highest T2 values, was scanned the same day, so it was only fixed for 5 hours. Out of these fixation times can be concluded that the longer the prostate was fixed, the lower the T2 values. This finding is consistent with literature, the study of McGrath *et al.* suggested that difference in T2 values between samples could be related to varying prostate volume and fixation time (67). In this study, there was no significant difference in prostate volume between the patients ($p=0.1944$) so the difference was most likely due to the difference in fixation time. However, fixation of tissue is important to preserve tissue from decomposition. In the future there can be suggested to standardize the fixation procedure to decrease the variability.

5.2.2.3. Correlation between the ADC values and the Gleason score

The Gleason scoring system has proven to be the most appropriate classification system in measuring the aggressiveness of the tumour, disease outcome and the risk of mortality of PCa (26). That is why in this study, the ADC and T2 values were correlated with the Gleason score. No significant correlation was found between the Gleason score and ADC values of the cancerous tissue in the PZ (p=0.084). Also for the T2 values and ADC values of the cancerous TZ no significant result was obtained by t-testing (T2: p=0.1354, ADC: p=0.0928). This negative result was maybe due to the little population size, as only 7 patients remained after exclusion of unsuitable data. In literature, a negative correlation is observed between the ADC values and Gleason score in different studies (68). In the study of Bourne *et al.* this negative correlation was also observed *in vivo*. The negative correlation was attributed to an increase in volume of low-diffusivity epithelial tissue and a concomitant decreasing volume of high-diffusivity stromal tissue and ductal space (69). The Gleason pattern is based on the architectural pattern of prostate tissue rather than the cell density. Therefore, the negative correlation between ADC values and Gleason score is, according to Chatterjee *et al.*, inferiorly correlated with the increased cell density (64).

In this study, the intension was to correlate the ADC and T2 values with the TNM stage. Unfortunately, only 14 patients were included in the study and after exclusion of the unsuitable data, only seven patients remained. Solely two different grades were present in the seven remainder patients. Only two patients had a TNM stages of 3a and all the other patients had a TNM stage of 2c, so a correlation would not be valuable. More patients data is required to correlate ADC and T2 values with the Gleason score or TNM stage, also including higher grade tumours.

5.2.2.4. Fractional anisotropy results

FA was tested as additional biomarker to distinguish low grade tumours that need more aggressive therapy from tumours where active surveillance is more appropriate. The *ex vivo* FA from healthy tissue was compared with cancerous lesions in the TZ and PZ separately (Figure 10). Significant differences were observed between healthy and cancerous tissue in the TZ (p=0.0004). In contrast to the PZ where no significant correlation was observed (p=0.2877). FA from the TZ and PZ was also compared to each other and no significant difference was obtained, not in the healthy tissue (p=0.3926) nor in tumour lesions (p=0.5168). These results are not consistent with literature, where significant differences were observed in FA between the PZ and TZ(70). This negative result is probably due to a little population size. The FA was only tested on 4 patients, the same patients as for the T2 values. This sample size was due to the very low resolution of the FA maps of the other patients. The low signal to noise ratio (SNR) made an accurate estimation of FA not possible. In the study of Bourne *et al.*, high FA was measured in fibromuscular stromal tissue, that was significantly higher than FA from epithelial tissue (65). A decrease in diffusivity is observed in cancerous tissue

due to loss in large ductal and luminal spaces (47). Simulations have shown that low SNR results in an overstimulation of FA, this means that an increase in FA in tumours is most likely due to low SNR rather than the presence of PCa. Therefore, Uribe *et al.* suggested that FA does not contribute to the diagnostic capabilities of diffusion tensor imaging in PCa (63).

5.3. Registration

A quantitative model to distinguish non-cancerous from cancerous regions on MR images would be ideal for the identification of biomarkers. However, it is difficult to directly delineate the extent of the disease on *in vivo* MR images, and that is why histology is still the gold standard (58).

5.3.1. Registration obstacles

Mapping the histology volume to the MRI volume, requires numerous degrees of freedom. Therefore, intermediate imaging stages are required to map the two datasets. For these intermediate imaging stages, different methods could be used. For example pictures that are made of the histological block before and after the H&E slice is cut with the microtome. However, these blockface images are time consuming and not clinical routine (62). Secondly, the prostate gland could also be scanned *ex vivo*. The advantage of this approach is that *ex vivo* imaging is motionless. Thanks to these intermediate steps, the histology data can be registered to the *in vivo* MRI stack with the *ex vivo* dataset as intermediate. This requires less degrees of freedom and reduced the bias and measurement errors (58). In this study, both intermediate techniques were used to register the MRI volume to the histology volume. First, macroslides of 3 mm were used instead of blockface images to make a 3D reconstruction of the prostate gland. Secondly, the prostate gland was scanned *ex vivo* which is motionless and has a high-resolution thanks to the 9.4T MRI unit. Thanks to high-resolution *ex vivo* imaging of the prostate gland (50 µm isotropic or below), *ex vivo* imaging provided extra information compared to *in vivo* MRI. An additional improvement of *ex vivo* MR scanning compared to conventional histology is that a complete dataset of the entire specimen is acquired in contrast to some arbitrarily chosen thin histology slices, as it was in the past. This high-resolution allows to identify potential hot spots for later histology. Thanks to the high-resolution, *ex vivo* MRI scanning tends towards virtual pathology.

DWI MR scans are suggested as the ideal method with a spatial resolution that is approaching cellular scale, according to Bourne *et al*. Currently, PCa is defined on tissue structure by histopathology, so a detection method that generates its contrast based on the structural tissue properties on microscopic level, would be expected to provide both sensitive and specific cancer detection (47). mpMRI has a spatial resolution that is approaching cellular scale, which makes it extremely valuable for the detection of PCa, but also for the identification of biomarkers.

5.3.2. Mold design

During the registration process, the histology images were registered to the *ex vivo* MR images and this was correlated to the *in vivo* MR images to map the spatial extent of the tumours. For the registration an exact correspondence is necessary between the MRI and the histology slices and therefore different sectioning devices were designed (71). In this study a precise one-to-one correlation between the *in vivo*, *ex vivo* MRI and histopathology data was possible thanks to the 3D mold which ensured the same slice thickness and orientation. This mold offers many benefits compared with the current specimen processing techniques. The mold is better compared to other devices because it is based on the *in vivo* shape of the prostate and it controls prostate deformation during slicing (66). In that way it reduces the geometric difference between the *in* and *ex vivo* data as much as possible. Thanks to the 3D mold design, the above mentioned limitations of registration can be overcome (72).

In this project, the patient-specific mold design was based on the first *in vivo* MRI scan. A point of attention is the time between the first MRI scan and the surgery. If the time period is too long, the prostate shape could change and then there is bigger chance that the prostate does not fit into the mold. For 4 of the 14 patients the mold did not fit. The mold of patient 1 was too big while that of patients 2, 11 and 13 was too small. This could be due to two different reasons. First, there is a difference between the prostate gland *in* and *ex vivo* caused by prostate deformation as previously described. Secondly, the time between the *in vivo* MRI scan and the operation can be too long so that the prostate grew and does not fit in the mold any longer.

My colleague, Simon Vanden Berghe, generated the molds for patients 12-14 and according to him the delineation itself of the prostate was very complex and difficult as it was not easy to distinct the outer prostate and the fatty or fibrous tissue around it. When surrounding tissue was included in the delineation, the prostate volume was overestimated, which may be a reason why the mold did not fit. Another suggested reason was that the segmentation tool that was used to do this, picked the widest delineation when the delineations were not overlapping perfectly in two different planes (60). To reduce the problem of unsuited molds, the delineation program can be adapted in such a way that it does not longer pick the widest delineation. Secondly, the time between the first scan and the surgery can be standardized or reduced to the minimum. Thirdly, an experienced radiologist must perform the delineation so that the least surrounding tissue is incorporated into the mold.

The mold design was updated after patient 6 to a more innovate design to diminish the rotational mispositioning of the prostate gland inside the mold as much as possible. The improved mold design contained urethra catheter guides which decreased mispositioning of the prostate gland into the mold. Secondly, infiltration holes were added so that the tissue could be fixated inside the mold to maintain its *in vivo* shape. Hereby possible deformation of the tissue and positioning difficulties due to fixation-induced rigidity were avoided. Liquid filled channels in the mold also provided landmarks visible on the *ex vivo* MR scans. Thanks to this mold design the *in vivo* and *ex vivo* MR images and H&E slides were acquired in the same orientation, plane and had the same slice thickness which made the registration of all these images a lot easier(73). By the deadline of the thesis, no articles were found with the same mold design.

Adequate registration of histopathological data to MRI findings is a crucial step for validation of mpMRI as a tool for diagnosing, localizing and grading low grade PCa (73). The two mostly used approaches in literature were both performed in this study to register histology to MRI data. On one hand the 3D histology stack reconstruction was registered to the 3D MR volume, and on the other hand each H&E slide was corresponded separately to the matching *ex vivo* MR slice.

5.3.2.1. Limitations of the 3D registration technique

A 3D histological reconstruction of the prostate gland was made based on the H&E slides. However, still some problems of the 3D registration technique are not solved yet to register the 3D MR volume to the 3D histology volume. The first problem is that the reconstruction of the 3D histology volume is not easy because when histopathological slides are made, often tissue gets loss or is distorted while cutting or H&E staining. This problem was solved by researchers via blockface images or manually placing control points (57,58,62). However, these solutions are both not realistic to execute for every patient for every slice as this is very time intensive and laborious for the pathologist. Moreover, in clinical practice this process must be performed in a reasonable timeframe. In our study macroslides of 3 mm were used instead of blockface images to make a 3D reconstruction of the prostate. Secondly, H&E slides of prostate specimens do not fit on regular histology glass slides. In other studies the prostate was cut up in four pieces to fit on normal glass slices. Thereafter a reconstruction to whole-mount sections was performed in Photoshop (4,61). In our study bigger glass slides were used, but sometimes the prostate gland was that big that the section was tilted to fit on the slide. This angle and the different orientations of the H&E slides within the same sample made it difficult to generate a 3D histology stack.

5.3.2.2. Limitations of the 2D registration technique

In the second registration approach, 2D H&E slice registration to the corresponding MRI slice, there must be an exact correspondence between a histology slice an a particular MRI slice. Thanks to our mold design 2D to 2D registration was possible. The histological artefacts however remain present as previously described. As solution for this problem, manually indicating landmarks is the most reliable and commonly used approach. The manual selection of these special landmarks is not easy on *ex vivo* MR images, even for experienced radiologists, and is a very time consuming and laborious task (57,58).

In this project, the prostate gland was cut up in the mold perpendicular to the urethra. This direction was important for further histopathological workup. A front-back mold design was tested on patient 12 to reduce the influence of prostate deformation but this was impossible to use because the cutting plane was different than normally used in histopathological workup. The H&E slide distortion was present in all cases. The problem of the tilting of the H&E slides on the glass slide was also faced. In the manual registration approach, the different angles of the H&E slides were adapted manually to be able to generate a 3D stack. The problem also occurred in the registration tool where the ROI in the Hist 2 ex/MB step was difficult to fit around the H&E slide when this was not parallel placed on the slide. This tilting problem can be solved with an additional registration step whereby the tilting of macroslides and H&E slides can be adapted manually. However, this does not stroke with the theoretical idea that the registration program is based on a limited degrees of freedom to make the program robust and trustable. The problems encountered during the histological workup may be solved by training and designating a pathologist for this study in particular.

The registration process of histopathological to MRI data needs further validation. The tilting of the H&E slides make it difficult to reconstruct a histological 3D volume and the histological artefacts are unavoidable in realistic clinical practice. That is why according to Xiao *et al.* the 2D registration method is the only approach that could accurately register histology to MRI data (62). However, as this is a very time-consuming and laborious work, automatic registration programs could improve the registration process. Only for patient 8 the registration was successful with the registration tool. Out of this experience can be concluded that the registration process needs validation.

5.4. Potential of mpMRI

The registration process needs validation as mpMRI is a very promising technique that could screen PCa patients non-invasively and it could guide biopsies. Accurate registration would clarify the information that is present in *in vivo* MRI scans and accurately localize tumour lesions which is very important in focussed treatment options like focal radiation therapy. mpMRI could address the detection of indolent tumours, as mentioned earlier. In this study, the idea was to determine a tumour size cut-off. In the study of Haider *et al.*, a tumour size cut-off was used of >4 mm² in diameter (74). In this study, the cut-off would be determined based on the resolution of the MRI scan. Two times the resolution in each direction would be the ideal cut-off size as below this size, partial-volume effects cannot be excluded. However, in this study the idea could not be tested practically as the resolution of the ADC maps was too low.

The goal of mpMRI research is to find biomarkers that can detect the extent, grade and molecularly assess the aggressiveness of PCa. However, with the current approach it is still difficult to identify low grade tumour by MRI. Further research could be focused on information provided by DW MRI scanning. For instance, anisotropy of diffusion namely DTI, FA and ADC values, non-Gaussian behaviour of diffusion, diffusion kurtosis and other non-mono-exponential fitting approaches of the diffusion data could provide more information to identify and grade low grade PCa (75).

Now mpMRI is already used in clinical practice in hospitals where an MRI unit is available, although it is not implemented yet in the EAU guidelines of 2015 (10). This is because treatment of PCa differs in European countries and an MRI unit is not always available. The guidelines indicate that mpMRI should be used for local staging of high grade PCa as it has an excellent sensitivity for PCa with a Gleason score >7. On the other hand, for low grade PCa, not many controlled trials are published yet. Some articles proposed mpMRI as a triage test for biopsy candidates to increase the detection of aggressive cancers and reduce over-detection. However, currently not enough evidence is gathered to recommend mpMRI before the first set of prostate biopsies. Therefore in this study, the purpose was to identify *in vivo* MRI biomarkers for low grade PCa to extent the clinical practice of mpMRI for low grade PCa.

5.5. Conclusion

Recently mpMRI has emerged as a promising non-invasive modality to detect PCa (39–41). mpMRI has shown to have an improved sensitivity and specificity compared to T2w MRI alone (37). Different acquisition protocols are used to capture multiple forms of information: functional information thanks to DCE, vascular information with DWI and structural information with T2w scans. The use of mpMRI in clinical practice for the detection and localization of PCa *in vivo* can have implications on image-guided biopsies, confocal radiotherapy and treatment of PCa (4). Now mpMRI is already used in clinical practice but it is not yet implemented in the EAU guidelines for the diagnosis, localization or treatment of PCa as it depends on the country, institution and availability of an MRI unit . It is important that the registration problems of histology to mpMRI are solved so that mpMRI can be validated and implemented in the standard of care. The aim of this project was to determine radiological signatures of PCa on *in vivo* and *ex vivo* MR images. In this study, ADC values of cancerous tissue were significantly lower than healthy tissue in the transition zone (65). To validate mpMRI, an accurate estimation of the real PCa extent is necessary on each of the imaging modalities. In this project a patient-specific, 3D printed mold was used that ensured a one-to-one correlation of the histology slices with the *in* and *ex vivo* MR images. Thanks to the 3D mold design, the registration of these images simplified as they were all acquired in the same plane and rotation. In this project the registration was performed by the two most common used approaches: first manual registration of the histology to *ex vivo* images, and secondly an in house designed registration software which registered the histology to the i*n vivo* MR images, with the high resolution *ex vivo* MR images as intermediate. *Ex vivo* MRI scanning and custom-printed 3D molds could not be used in clinical practice as this is too expensive and time consuming, but it can provide the necessary research information for the validation of mpMRI (58). If the automatic registration tool that is used in this study is more validated, histology images could be adequately correlated with MR images to accurately localize prostate lesions. This is important for the validation of mpMRI. If so, mpMRI would have broad clinical implications including tumour detection, grading and localization via non-invasive imaging, but also treatment selection, MRI-targeted biopsies, preoperative planning and follow-up for active surveillance for low grade PCa (4).

6. Nederlandstalige samenvatting

Prostaatkanker (PCa) is de meest voorkomende kanker bij oudere mannen (>70 jaar) in Europa (10). Ongeveer 417 000 patiënten werden gediagnosticeerd met PCa in 2012, wat wil zeggen dat één man op zes geconfronteerd wordt met PCa gedurende zijn leven (1). Door dit hoge aantal is er heel wat onderzoek gefocust op het vinden van niet-invasieve manieren om PCa te diagnosticeren. Momenteel wordt de diagnose gesteld met behulp van biopsies die genomen worden onder begeleiding van transrectale echografie (8). Daarbij worden meerdere biopsies genomen om een inschatting te kunnen maken over de uitgebreidheid van de kanker en de graad. De eigenlijke diagnose wordt dan gesteld op basis van histopathologische analyse van deze biopsies. Dit is echter een zeer pijnlijk onderzoek, wat zou kunnen verholpen worden door niet-invasieve technieken voor de diagnose van prostaatkanker. Multi-parametrische magnetische resonantie beeldvorming (mpMRI) zou kunnen bijdragen als niet invasieve beeldvormingstechniek in dit probleem omdat er meerdere scan protocollen gecombineerd worden waardoor zowel anatomische als functionele informatie bekomen wordt (5,37). mpMRI zou behulpzaam kunnen zijn bij de diverse behandelingsstadia van PCa. Bijvoorbeeld biopsies onder leiding van MRI, het detecteren en diagnosticeren van PCa, het plannen van chirurgische procedures, het optimaal plannen van de behandeling evenzeer als de evolutie van PCa opvolgen (4). Momenteel is mpMRI al geïmplementeerd in de klinische praktijk maar het is nog niet standaard zorg en ook nog niet opgenomen in de Europese associatie van urologie (EAU) richtlijnen van 2015 (10). mpMRI zou echter kunnen bijdragen in het kiezen van de optimale behandeling. Zo kan het laaggradige patiënten begeleiden om meer te kiezen voor actieve opvolging in plaats van chirurgie (21). Dit kan de levenskwaliteit van patiënten aanzienlijk verhogen en de financiële impact op de maatschappij reduceren (58). Voordat mpMRI volledig kan geïmplementeerd worden in de klinische praktijk moet er echter nog verdere validatie gebeuren van deze techniek. Daarom is het doel van deze studie om biomarkers te vinden voor laaggradige tumoren op *in vivo* MRI beelden. Om dit te kunnen doen werden laaggradige patiënten geïncludeerd in de studie die gepland waren voor een robotoperatie. Twee *in vivo* MRI scans werden uitgevoerd en na de chirurgische verwijdering van de prostaat werd deze nogmaals gescand *ex vivo* met een sterkere MRI scanner. Daarna werd de klassieke histologische behandeling verder gezet. De *in vivo* MRI beelden werden geregistreerd met de *ex vivo* MRI beelden en de histologische coupes om zo biomarkers te bepalen voor laaggradige tumoren.

6.1. Huidige diagnose en behandeling van prostaatkanker

De diagnose van prostaatkanker wordt op heden gesteld door een combinatie van PSA niveau, palpatie van de prostaat en biopsies (10). In eerste instantie wordt door middel van een bloedafname het prostaat specifiek antigen (PSA) niveau gemeten. Dit proteïne wordt aangemaakt door de prostaat en kan verhoogd zijn bij prostaatkanker (24). Indien een verhoogde PSA waarde wordt vastgesteld, >4 ng/ml, wordt een palpatie van de prostaat uitgevoerd om na te gaan of er oneffenheden in de prostaat worden gevoeld. Indien dit positief is, kunnen biopsies onder leiding van echografie uitsluitsel geven over de diagnose, de graad en uitgebreidheid (10). Indien prostaatkanker wordt vastgesteld, zijn er verschillende behandelingsopties mogelijk. Ten eerste kan er geopteerd worden voor actieve follow-up van de tumor zonder invasieve therapie (30). Als er dan echter een uitbreiding van huidige status wordt vastgesteld, kan er nog altijd overgeschakeld worden naar meer ingrijpende behandelingsopties. De klassieke behandelingen daarbij zijn chirurgie, radiotherapie en chemotherapie. Daarnaast kan bij prostaatkanker ook hormonale therapie geopteerd worden waarbij het testosteron niveau drastisch verlaagd wordt, wat de groei van tumoren remt (10).

De laatste 10 jaar zijn er meer en meer PSA screenings gebeurd waardoor ook onschuldige tumoren ontdekt worden. Dit stelt echter een ethisch dilemma, moeten deze tumoren behandeld worden of niet. De kans op overbehandeling stijgt daarbij aanzienlijk en het zorgt voor een verhoogde financiële kost (58). Het is momenteel echter moeilijk om een onderscheid te maken tussen laaggradige tumoren waarbij actieve opvolging een betere keuze is of tumoren waarvoor een agressievere behandeling meer optimaal is.

Het doel van deze studie was dan ook om patiënten met laaggradige tumoren te includeren om, op basis van mpMRI beelden, biomarkers te kunnen bepalen die het onderscheid tussen onschuldige en agressieve tumoren kunnen helpen inschatten.

6.2. Multiparametrisch MRI

Multiparametrische MRI combineert verschillende scan protocollen om dan deze functionele en anatomische informatie te gebruiken om prostaatkanker tumoren te lokaliseren (4). Hierbij maken dynamisch contrast versterkte beelden (DCE), T2 gewogen beelden (T2w) en diffusie gewogen beelden (DWI) deel uit van het mpMRI protocol. Ten eerste, DCE scans maken gebruik van contrastvloeistoffen om de biologische kenmerken van tumoren te bekijken (36). De snelheid van de opname en afvloei van de contrastvloeistof geeft informatie over de functionele kenmerken van de tumor. Ten tweede, T2 gewogen beelden hebben een hoge resolutie en bieden anatomische en structurele informatie omtrent de prostaat (76). Ten derde, diffusie gewogen beelden bieden vasculaire informatie. Hierbij wordt gekeken naar de diffusie van water, wat kan beperkt zijn in

tumoren omdat deze een densere structuur hebben. Diffusie kan informatie bieden over de densiteit van het weefsel wat dan de laesie verder karakteriseert (21,65). De voorgaande drie technieken samen zorgen dankzij de combinatie van zowel anatomische als functionele informatie voor een meer accurate diagnose van prostaatkanker met behulp van MRI.

MpMRI wordt momenteel al gebruikt in klinische praktijk maar in de EAU richtlijnen wordt het gebruik van mpMRI enkel gesuggereerd voor hooggradige PCa (10). Om dit verder uit te kunnen breiden naar laaggradige tumoren, werden in deze studie 14 patiënten geïncludeerd met laaggradige tumoren om MRI biomarkers vast te kunnen stellen (57,58). Dit kan helpen in het valideren van de techniek en het implementeren van mpMRI in de standaard zorg.

Momenteel moeten bevindingen op basis van de MRI beelden nog gevalideerd worden door middel van histologie (5,57,58). Een goede registratie van de MRI beelden met de histologische resultaten vormt echter een obstakel daarbij. In deze studie is daarom een patiënt-specifieke mal gemaakt die 3D wordt geprint om zo een goede registratie van alle beelden te kunnen garanderen. Deze mal bevat verschillende voordelen in vergelijking met de huidige hulpmiddelen die al op de markt zijn (72). Zo is een uitsparing voor de in- en uitgang van de urethra toegevoegd aan het ontwerp van de mal om zo een verkeerde positionering van de prostaat tot het minimum te reduceren. Daarnaast bevat de mal parallelle gleuven om de 3 mm waardoor de prostaat kan worden opgesneden in de mal voor histologisch onderzoek, wat perfect parallelle coupes op de gewenste afstand garandeert. Verder zijn openingen gecreëerd in de mal zodat de prostaat kan gefixeerd worden in de mal zelf wat ervoor zorgt dat de *in vivo* vorm behouden blijft (72). Dankzij het design van deze mal worden de *in vivo* en *ex vivo* MRI beelden samen met de histologische coupes perfect in hetzelfde vlak gemaakt en met dezelfde oriëntatie wat de registratie van deze beelden vereenvoudigt.

6.3. Resultaten van de studie

Veertien patiënten werden prospectief geïncludeerd in de studie met laaggradige PCa. De gemiddelde leeftijd van deze patiënten was 68 jaar met een gemiddeld PSA niveau van 10,46 ng/ml. De tumorstadia in deze patiëntenpopulatie varieerde van een TNM stadium 2a tot 3a, waarvan 88% van de tumoren gelokaliseerd waren in de perifere zone (PZ) van de prostaat.
De registratie van de beelden werd op twee manieren uitgevoerd. Ten eerste, een manuele registratie van de MRI beelden met de corresponderende histologische coupe. Daarvoor was de mal noodzakelijk om een 1 op 1 correlatie te kunnen garanderen tussen de beelden. Daarnaast werd ook een registratie tool ontwikkeld waarbij de MRI beelden automatisch konden geregistreerd worden met de histologische data, de *ex vivo* MRI beelden werden hierbij gebruikt als tussenstap.

Op basis van deze geregistreerde beelden werden T2 waarden en ‘apparent diffusion coefficient’ (ADC) waarden bepaald om zo een biomarker te kunnen bepalen voor laaggradige tumoren.

Er werd een significant verschil aangetoond tussen de ADC waarden van gezond en kankerweefsel in de transitie zone (TZ) ($p<0.0001$). Er werd echter geen significant verschil gevonden in de ADC waarden van de PZ of de T2 waarden van zowel de TZ als de PZ. In de literatuur wordt dit resultaat van lagere ADC waarden in tumoren in vergelijking met gezond weefsel bevestigd, zowel *in* als *ex vivo* (55,64,77). Deze lagere ADC waarden duiden op een verminderde mobiliteit van water in tumoren en een verhoogde cel densiteit (59).

Daarnaast werd wel een correlatie waargenomen tussen de grootte van de T2 en ADC waarden en de grootte van de afgelijnde regio. Hierbij werd geconstateerd dat hoe groter de afgelijnde regio was, hoe hoger de T2 waarden waren en hoe lager de ADC waarden.

Bij het uitzetten van de T2 en ADC waarden per zone, werden verschillende groepen waargenomen. Deze groepvorming kwam overeen met verschillende patiënten. Dit significant verschil in T2 en ADC waarden per patiënt kan verklaard worden door een verschil in fixatieduur. Dit is consistent met de studie van McGrath *et al.* waarbij er een verschil in T2 waarden geobserveerd werd tussen verschillende stalen (67). Dit werd toegeschreven aan een verschillende fixatieduur of een verschil in prostaatvolume.

In deze studie werd geen significante correlatie gevonden tussen de ADC waarden en de Gleason score, die wordt gebaseerd op histologische stalen en bepaalt hoe verschillend het tumorweefsel is van gezond weefsel. In tegenstelling tot de literatuur waar de Gleason score negatief gecorreleerd is met ADC waarden. Deze negatieve correlatie wordt toegeschreven aan de verminderde mobiliteit van water in tumoren zoals hierboven al beschreven werd (57,71). Deze negatieve correlatie kon hier wellicht niet aangetoond worden door een te kleine testgroep.

Als andere biomarker werd ook nog gekeken naar de fractionele anisotropie (FA). Een significant verschil in FA tussen gezond en kankerweefsel werd gezien in de TZ ($p=0.0004$). Dit was echter niet het geval in de PZ. Ook werd er geen significant verschil waargenomen tussen de TZ en PZ onderling. Dit in tegenstelling tot de literatuur waar de FA van de PZ significant lager is dan van de TZ (63). Dit verschil wordt toegeschreven aan de verminderde diffusiviteit in tumoren doordat de hoeveelheid epitheel toeneemt (wat een lage diffusivititeit heeft) en het percentage stroma en ductale ruimte afneemt (wat een hoge diffusiviteit heeft) (69).

6.4. Conclusie

Uit deze studie kan geconcludeerd worden dat het registratieproces verdere validatie nodig heeft. Het automatisch registratie programma werkte maar voor 1 patiënt en de manuele registratie is zeer tijdrovend. Als de registratie van histologische beelden en MRI beelden geoptimaliseerd is, kan dit zorgen voor validatie van mpMRI (76). mpMRI is een zeer veelbelovende techniek waarmee PCa patiënten niet-invasief kunnen gescreend worden en biopsies kunnen begeleid worden (57). Een accurate registratie kan de informatie die aanwezig is op *in vivo* MRI beelden verder verduidelijken en tumoren accuraat lokaliseren, wat zeer belangrijk is in gerichte behandelingen zoals focale radiotherapie (37). mpMRI kan ook het ethische dilemma van de onschuldige tumoren aanpakken zoals eerder vermeld (58). Het doel van de studie was om biomarkers te vinden die de omvang, graad en agressiviteit van laaggradige tumoren kunnen inschatten (10,24,56). De verlaagde ADC waarden in tumoren zijn daar een voorbeeld van (64). Er is echter verder onderzoek nodig met een grotere patiëntenpopulatie om de resultaten uit deze studie te bevestigen. Het design van die 3D mal die in deze studie ontworpen is, heeft veel voordelen in vergelijking met de huidige registratie hulpmiddelen (72). Het gebruik van deze 3D mallen kan echter niet geïmplementeerd worden in de klinische praktijk omdat dit te tijdrovend en te duur is. Het kan daarentegen wel de nodige informatie bezorgen uit klinisch onderzoek die nodig is voor de validatie van mpMRI voor laaggradige tumoren. Als mpMRI gevalideerd is, dankzij deze 3D mal en het automatisch registratieprogramma, dan kan dit vergaande klinische gevolgen hebben zoals tumor detectie en lokalisatie via niet-invasieve technieken maar ook op vlak van behandelingskeuze, MRI begeleide biopsies, preoperatieve planning en follow-up van patiënten met laaggradige PCa (4).

References

1. Bray F, Lortet-Tieulent J, Ferlay J, Forman D, Auvinen A. Prostate cancer incidence and mortality trends in 37 European countries: an overview. Eur J Cancer. 2010;46(17):3040–52.
2. Miller, Rebecca L. Siegel KD, , Ahmedin Jemal D. Cancer Statistics, 2016. CA Cancer J Clin. 2016;66(1):7–30.
3. Trivedi H, Turkbey B, Rastinehad AR, Benjamin CJ, Bernardo M, Pohida T, et al. Use of patient-specific MRI-based prostate mold for validation of multiparametric MRI in localization of prostate cancer. Urology. 26;79(1):233–9.
4. Orczyk C, Mikheev A, Rosenkrantz AB, Melamed J, Taneja SS, Rusinek H. Imaging of prostate cancer: a platform for 3D co-registration of in-vivo MRI ex-vivo MRI and pathology. Proc SPIE--the Int Soc Opt Eng. 2012;8316:83162.
5. Priester A, Natarajan S, Le JD, Garritano J, Radosavcev B, Grundfest W, et al. Original Article A system for evaluating magnetic resonance imaging of prostate cancer using patient-specific 3D printed molds. Am J Clin Exp Urol. 2014;2(2):127–35.
6. Bhavsar A, Verma S. Anatomic imaging of the prostate. Biomed Res Int. 2014 Jan;2014:9.
7. Heidenreich A. New Developments in the Management of Prostate Cancer. Oncol Res Treat. 2015;38(38):628.
8. Heidenreich A, Bellmunt J, Bolla M, Joniau S, Mason M, Matveev V, et al. EAU guidelines on prostate cancer. Part 1: screening, diagnosis, and treatment of clinically localised disease. Eur Urol. 2011;59(1):61–71.
9. Date P. Incidence Fact Sheet Prostate Cancer Belgium 2013 Publication Date : 2015.
10. N. Mottet, J. Bellmunt EB, R.C.N. van den Bergh, M. Bolla, N.J. van Casteren, P. Cornford, S. Culine, S. Joniau, T. Lam, M.D. Mason, V. Matveev, H. van der Poel, T.H. van der Kwast, O. Rouvière TW. EAU-Guidelines-on-Prostate-Cancer-2015. European association of Urology. 2015.
11. Chustecka Z. Cancer Survival Rates Improving Across Europe, But Still Lagging Behind US [Internet]. Medscape medical news. 2007 [cited 2015 Nov 15]. Available from: http://www.medscape.com/viewarticle/561737
12. Bratt O. Hereditary Prostate Cancer: Clinical Aspects. J Urol. 2002;168(3):906–13.
13. OLA BRATT. Hereditary PCa. J Urol [Internet]. 2002;168:906–13. Available from: http://ac.els-cdn.com/S0022534705645417/1-s2.0-S0022534705645417-main.pdf?_tid=c82259cc-637c-11e5-997a-00000aab0f02&acdnat=1443182509_147504c50ba1616a2e34a8e3a2709ae7
14. Grönberg H. Prostate cancer epidemiology. Lancet. 2003;361(9360):859–64.
15. Board PATE. Prostate Cancer Treatment (PDQ®) [Internet]. National Cancer Institute (US); 2015 [cited 2015 Sep 25]. Available from: http://www.ncbi.nlm.nih.gov/books/NBK66036/
16. Thompson IM, Ankerst DP, Chi C, Goodman PJ, Tangen CM, Lucia MS, et al. Assessing prostate cancer risk: Results from the Prostate Cancer Prevention Trial. J Natl Cancer Inst. 2006;98(8):529–34.

17. Lee CH, Akin-Olugbade O, Kirschenbaum A. Overview of prostate anatomy, histology, and pathology. Endocrinol Metab Clin North Am. 2011;40(3):565–75, viii – ix.

18. Winslow T. Prostate Cancer Treatment—Health Professional Version - National Cancer Institute [Internet]. 2005 [cited 2015 Dec 10]. Available from: http://www.cancer.gov/types/prostate/hp/prostate-treatment-pdq#link/_1682_toc

19. Wang S, Burtt K, Turkbey B, Choyke P, Summers RM. Computer Aided-Diagnosis of Prostate Cancer on Multiparametric MRI: A Technical Review of Current Research. Biomed Res Int. Hindawi Publishing Corporation; 2014;1–11.

20. Horwich A, Parker C, Bangma C, Kataja V. Prostate cancer: ESMO Clinical Practice Guidelines for diagnosis, treatment and follow-up. Ann Oncol [Internet]. 2010 May 1 [cited 2015 Aug 20];21 Suppl 5(suppl 5):v129–33. Available from: http://annonc.oxfordjournals.org/content/21/suppl_5/v129.full

21. Richenberg J, Clements R, Verma S, Villeirs G, Rouviere O, Logager V, et al. ESUR prostate MR guidelines 2012. Eur Radiol. 2012;22(4):746–57.

22. Nash PA, Bruce JE, Indudhara R, Shinohara K. Transrectal ultrasound guided prostatic nerve blockade eases systematic needle biopsy of the prostate. J Urol. 1996;155(2):607–9.

23. Nazir B. Pain during transrectal ultrasound-guided prostate biopsy and the role of periprostatic nerve block: what radiologists should know. Korean J Radiol. 2014;15(5):543–53.

24. Payne H, Cornford P. Prostate-specific antigen: an evolving role in diagnosis, monitoring, and treatment evaluation in prostate cancer. Urol Oncol.; 2009;29(6):593–601.

25. Hricak H, Scardino P. Prostate Cancer. NCCN Guidelines. 2009. p. 60.

26. Hambrock T, Hoeks C, Hulsbergen-Van De Kaa C, Scheenen T, Fütterer J, Bouwense S, et al. Prospective assessment of prostate cancer aggressiveness using 3-T diffusion-weighted magnetic resonance imaging-guided biopsies versus a systematic 10-core transrectal ultrasound prostate biopsy cohort. Eur Urol. 2012;61(1):177–84.

27. Woodfield C a., Tung G a., Grand DJ, Pezzullo J a., Machan JT, Renzulli JF. Diffusion-weighted MRI of peripheral zone prostate cancer: Comparison of tumor apparent diffusion coefficient with Gleason score and percentage of tumor on core biopsy. Int Braz J Urol. 2010;36:316–22.

29. Edge, S., Byrd, D.R., Compton, C.C., Fritz, A.G., Greene, F.L., Trotti A. AJCC Cancer Staging Manual | Stephen Edge | Springer. Seventh ed. Springer, 2010. 648 p.

30. Johnson LM, Choyke PL, Figg WD, Turkbey B. The Role of MRI in Prostate Cancer Active Surveillance. Biomed Res Int. Hindawi Publishing Corporation; 2014;1–6.

31. Dall'Era MA, Konety BR, Cowan JE, Shinohara K, Stauf F, Cooperberg MR, et al. Active surveillance for the management of prostate cancer in a contemporary cohort. Cancer. 2008;112(12):2664–70.

32. Al Otaibi M, Ross P, Fahmy N, Jeyaganth S, Trottier H, Sircar K, et al. Role of repeated biopsy of the prostate in predicting disease progression in patients with prostate cancer on active surveillance. Cancer. 2008;113(2):286–92.

33. Rider JR, Sandin F, Andrén O, Wiklund P, Hugosson J, Stattin P. Long-term outcomes

among noncuratively treated men according to prostate cancer risk category in a nationwide, population-based study. Eur Urol. 2013;63(1):88–96.

34. Bill-Axelson Anna, Holmberg Lars MR, Häggman Michael, Swen-Olof Andersson et al. Radical Prostatectomy versus Watchful Waiting in Early Prostate Cancer [Internet]. N Engl J Med. 2011 [cited 2015 Nov 15]. p. 352(19):1977–84. Available from: http://www.nejm.org/doi/pdf/10.1056/NEJMoa043739

35. De Carlo F, Celestino F, Verri C, Masedu F, Liberati E, Di Stasi SM. Retropubic, laparoscopic, and robot-assisted radical prostatectomy: surgical, oncological, and functional outcomes: a systematic review. Urol Int. 2014;93(4):373–83.

36. Borren A, Groenendaal G, Moman MR, Boeken Kruger AE, van Diest PJ, van Vulpen M, et al. Accurate prostate tumour detection with multiparametric magnetic resonance imaging: dependence on histological properties. Acta Oncol. 2014;53(1):88–95.

37. Isebaert S, Van Den Bergh L, Haustermans K, Joniau S, Lerut E, De Wever L, et al. Multiparametric MRI for prostate cancer localization in correlation to whole-mount histopathology. J Magn Reson Imaging. 2013;37(6):1392–401.

38. Akin O, Sala E, Moskowitz CS, Kuroiwa K, Ishill NM, Pucar D, et al. Transition zone prostate cancers: features, detection, localization, and staging at endorectal MR imaging. Radiology. 2006;239(3):784–92.

39. Kuru TH, Van Essen J, Pfister D, Porres D. Role of Focal Therapy with High-Intensity Focused Ultrasound in the Management of Clinically Localized Prostate Cancer. Oncol Res Treat. 2015;38:634–8.

40. Orczyk C, Rusinek H, Rosenkrantz AB, Mikheev A, Deng F-M, Melamed J, et al. Preliminary experience with a novel method of three-dimensional co-registration of prostate cancer digital histology and in vivo multiparametric MRI. Clin Radiol.;68(12):e652–8.

41. Bratan F, Niaf E, Melodelima C, Chesnais AL, Souchon R, Mège-Lechevallier F, et al. Influence of imaging and histological factors on prostate cancer detection and localisation on multiparametric MRI: A prospective study. Eur Radiol. 2013;23(7):2019–29.

42. Schild PDHH. MRI made easy. volume 1. Berlin: Schering AG; 1990. 105 p.

43. Turkbey B, Pinto P a, Mani H, Bernardo M, Pang Y, McKinney YL, et al. Prostate cancer: value of multiparametric MR imaging at 3 T for detection--histopathologic correlation. Radiology. 2010;255(1):89–99.

44. Tofts PS. T1-weighted DCE Imaging Concepts : Modelling , Acquisition and Analysis. MAGNETOM Flash. 2010;1–5.

45. Moore CM, Ridout A, Emberton M. The role of MRI in active surveillance of prostate cancer. Curr Opin Urol. 2013;23(3):261–7.

46. Westphalen AC, Coakley F V, Kurhanewicz J, Reed G, Zhen J, Simko JP. Spectroscopy Features. AJR Am J Roentgenol. 2010;193(3):238–43.

47. Bourne R, Kurniawan N, Cowin G, Sved P, Watson G. 16 T Diffusion microimaging of fixed prostate tissue: Preliminary findings. Magn Reson Med. 2011;66(1):244–7.

48. Oto A, Yang C, Kayhan A, Tretiakova M, Antic T, Schmid-Tannwald C, et al. Diffusion-weighted and dynamic contrast-enhanced MRI of prostate cancer: Correlation of

quantitative MR parameters with gleason score and tumor angiogenesis. Am J Roentgenol. 2011;197(6):1382–90.

49. Miao H, Fukatsu H, Ishigaki T. Prostate cancer detection with 3-T MRI: comparison of diffusion-weighted and T2-weighted imaging. Eur J Radiol. 2007;61(2):297–302.

50. Weinreb JC, Barentsz JO, Choyke PL, Cornud F, Haider MA, Macura KJ, et al. PI-RADS Prostate Imaging - Reporting and Data System: 2015, Version 2. Eur Urol [Internet]. 2015 Sep 28 [cited 2015 Oct 20];69(1):16–40. Available from: http://www.ncbi.nlm.nih.gov/pubmed/26427566

51. Shah V, Pohida T, Turkbey B, Mani H, Merino M, Pinto PA, et al. A method for correlating in vivo prostate magnetic resonance imaging and histopathology using individualized magnetic resonance-based molds. Rev Sci Instrum. 2009;80(10):104301.

52. McGrath DM, Foltz WD, Al-Mayah A, Niu CJ, Brock KK. Quasi-static magnetic resonance elastography at 7 T to measure the effect of pathology before and after fixation on tissue biomechanical properties. Magn Reson Med. 2012;68(1):152–65.

53. Chappelow J, Bloch BN, Rofsky N, Genega E, Lenkinski R, DeWolf W, et al. Elastic registration of multimodal prostate MRI and histology via multiattribute combined mutual information. Med Phys. 2011;38(4):2005–18.

54. Turkbey B, Mani H, Shah V, Rastinehad AR, Bernardo M, Pohida T, et al. Multiparametric 3T prostate magnetic resonance imaging to detect cancer: histopathological correlation using prostatectomy specimens processed in customized magnetic resonance imaging based molds. J Urol. 2011;186(5):1818–24.

55. Xiao G, Bloch BN, Chappelow J, Genega EM, Rofsky NM, Lenkinski RE, et al. Determining histology-MRI slice correspondences for defining MRI-based disease signatures of prostate cancer. Comput Med Imaging Graph.; 2011;35(7-8):568–78.

56. Chaitanya Kalavagunta, MS, MS, MSc1, Xiangmin Zhou, PhD2, Stephen C. Schmechel M, PhD3, and Gregory J. Metzger P. Registration of in vivo Prostate MRI and Pseudo-Whole Mount Histology using Local Affine Transformations guided by Internal Structures (LATIS). J Magn Reson Imaging. 2015;73(4):389–400.

57. Orczyk, Clement, Taneja Samir S, Rusinek Henry RAB. Assessement of Change in Prostate Volume and Shape Following Surgical Resection Through Co-registration of In Vivo MRI and Fresh Specimen Ex Vivo MRI. Clin Radiol. 2015;2(2):398–403.

58. Fomby P, Cherlin AJ. Challenges in accurate registration of 3D medical imaging and histopathology in primary prostate cancer. Eur J Nucl MEd Mol Imaging. 2011;72(2):181–204.

59. Delongchamps NB, Rouanne M, Flam T, Beuvon F, Liberatore M, Zerbib M, et al. Multiparametric magnetic resonance imaging for the detection and localization of prostate cancer: Combination of T2-weighted, dynamic contrast-enhanced and diffusion-weighted imaging. BJU Int. 2011;107(9):1411–8.

60. Vanden Berghe S. Assessment of Prostate Tumors using High Resolution In Vivo and Ex Vivo MRI. 2016.

61. Haider MA, van der Kwast TH, Tanguay J, Evans AJ, Hashmi A-T, Lockwood G, et al. Combined T2-Weighted and Diffusion-Weighted MRI for Localization of Prostate Cancer. Am J Roentgenol. American Roentgen Ray Society; 2007;189(2):323–8.

62. Xiao G, Bloch BN, Chappelow J, Genega EM, Rofsky NM, Lenkinski RE, et al. Determining histology-MRI slice correspondences for defining MRI-based disease signatures of prostate cancer. Comput Med Imaging Graph; 2011;35(7-8):568–78.

63. Uribe CF, Jones EC, Chang SD, Goldenberg SL, Reinsberg SA, Kozlowski P. In vivo 3T and ex vivo 7T diffusion tensor imaging of prostate cancer: Correlation with histology. Magn Reson Imaging. 2015 Jun;33(5):577–83.

64. Chatterjee A, Watson G, Myint E, Sved P, McEntee M, Bourne R. Changes in epithelium, stroma, and lumen space correlate more strongly with gleason pattern and are stronger predictors of prostate ADC changes than cellularity metrics1. Radiology [Internet]. 2015;277(3):751–62.

65. Bourne RM, Kurniawan N, Cowin G, Sved P, Watson G. Microscopic diffusion anisotropy in formalin fixed prostate tissue: Preliminary findings. Magn Reson Med. 2012;68(6):1943–8.

66. Trivedi H, Turkbey B, Rastinehad AR, Benjamin CJ, Bernardo M, Pohida T, et al. Use of patient-specific MRI-based prostate mold for validation of multiparametric MRI in localization of prostate cancer. Urology 2012 Jan;79(1):233–9.

67. McGrath DM, Foltz WD, Brock KK. Measuring the Effect of Formalin Fixation on Ex Vivo Tissue Material Properties using High Resolution 3D Quasi-Static MR Elastography at 7 Tesla for Improved Biomechanical Registration of Histopathology , and Correlation with the Effect of Fixation on T 1. Proc Intl Soc Mag Reson Med. 2010;18:640.

68. Metrics C, Watson G. and Lumen Space Correlate More Strongly with Gleason Pattern and Are Stronger Predictors of Prostate ADC Changes than. 2015;000(0):1–12.

69. Bourne RM, Kurniawan N, Cowin G, Stait-Gardner T, Sved P, Watson G, et al. Microscopic diffusivity compartmentation in formalin-fixed prostate tissue. Magn Reson Med. 2012;68(2):614–20.

70. Bourne RM, Bongers A, Chatterjee A, Sved P, Watson G. Diffusion anisotropy in fresh and fixed prostate tissue ex vivo. Magn Reson Med. 2015 Oct 7;

71. Chen LH, Ho H, Lazaro R, Thng CH, Yuen J, Ng WS, et al. Optimum slicing of radical prostatectomy specimens for correlation between histopathology and medical images. Int J Comput Assist Radiol Surg. 2010;5(5):471–87.

72. Trivedi H, Turkbey B, Rastinehad AR, Benjamin CJ, Bernardo M, Pohida T, et al. Use of patient-specific MRI-based prostate mold for validation of multiparametric MRI in localization of prostate cancer. Urology.; 2012;79(1):233–9.

73. Elen An, Isebaert Sofie, De Keyzer Frederik, Himmelreich Uwe, Joniau Steven, Tosco Lorenzo, Dresselaers Tom, Lerut Evelyne, Oyen Raymond, Bourne Roger, Maes Frederik HK. Validation and workflow of an improved patient-specific mold design for registration of in-vivo MRI and histology of the prostate.

74. Haider MA, Van Der Kwast TH, Tanguay J, Evans AJ, Hashmi AT, Lockwood G, et al. Combined T2-weighted and diffusion-weighted MRI for localization of prostate cancer. Am J Roentgenol. 2007;189(2):323–8.

75. Bourne RM, Kurniawan N, Cowin G, Stait-Gardner T, Sved P, Watson G, et al. Biexponential diffusion decay in formalin-fixed prostate tissue: Preliminary findings. Magn Reson Med. 2012;68(3):954–9.

76. Fan X, Haney CR, Agrawal G, Pelizzari CA, Antic T, Eggener SE, et al. High-resolution MRI of excised human prostate specimens acquired with 9.4T in detection and identification of cancers: validation of a technique. J Magn Reson Imaging. 2011;34(4):956–61.

77. Ferlay J, Steliarova-foucher E, Lortet-tieulent J, Rosso S. Cancer incidence and mortality patterns in Europe : Estimates for 40 countries in 2012. Eur J Cancer. 2013;49(6):1374–403.

78. Harnden P, Shelley MD, Coles B, Staffurth J, Mason MD. Should the Gleason grading system for prostate cancer be modified to account for high-grade tertiary components? A systematic review and meta-analysis. Lancet Oncol.; 2007;8(5):411–9.